MLL regulates actin cytoskeleton and cell migration by stabilizing Rho GTPases via the transcription of RhoGDI1

Akash Nitin Chinchole[1,2], Kaisar Ahmed Lone[1,3], and Shweta Tyagi[1,*]

[1]Laboratory of Cell Cycle Regulation, Centre for DNA Fingerprinting and Diagnostics (CDFD), Uppal, Hyderabad 500039, India
[2]Graduate Studies, Manipal Academy of Higher Education, Manipal 567104, India
[3]Graduate Studies, Regional Centre for Biotechnology, Faridabad 121001, India

*Corresponding author: Laboratory of Cell Cycle Regulation, CDFD Uppal, Hyderabad 500039, India Email: shweta@cdfd.org.in
Phone: +91-40-27216115
Fax: +91-40-27216006

Abstract

Attainment of proper cell shape and regulation of cell migration are essential processes in development of an organism. Mixed lineage leukemia (MLL) protein, a H3K4 histone methyltransferase, plays critical role in cell-fate decisions during skeletal development and haematopoiesis in higher vertebrates. Rho GTPases—RhoA, Rac1 and CDC42—are small G proteins that regulate various key cellular processes like actin cytoskeleton formation, maintenance of cell shape, and cell migration etc. Here we report that MLL regulates the homeostasis of these small Rho GTPase. Loss of MLL results in abnormal cell shape and disrupted actin cytoskeleton, that leads to diminished cell spreading and migration. MLL depletion affects the stability and activity of Rho GTPases in SET domain-dependent manner, but these Rho GTPases are not direct transcriptional targets of MLL. Instead, MLL regulates the transcript levels of their chaperone protein RhoGDI1. Using MDA-MB-231, a triple negative breast cancer cell line with high RhoGDI1 expression, we show that MLL depletion

or inhibition by small molecule reduces tumour progression in nude mice. Our studies highlight the central regulatory role of MLL in Rho/Rac/CDC42 signalling pathways.

Introduction

Actin exists as a monomeric soluble form as well as filamentous form in the cells. The assembly of actin monomers into filaments or polymerization is brought about by proteins that belong to a family of 23 small G proteins called Rho GTPases. This assembly provides the cells with a strong mechanical framework due to which cells can migrate, maintain a rigid shape and transport cargo (Pollard and Cooper, 2009).

Rho family of GTPases contains small G proteins that act as molecular switches. Most of them are 'ON' when in GTP bound state and after GTP hydrolysis they switch back to 'OFF' state(Goitre *et al.*, 2014). Rho GTPases play an important role in regulating the dynamics of actin cytoskeleton, cell adhesion, establishing cell polarity and cell migration. Out of these, three GTPases are the best characterized, namely, RhoA, Rac1 and CDC42, each having unique as well as interdependent roles in signal transduction (Jaffe and Hall, 2005). Constitutively active mutants of RhoA, Rac1 and CDC42 gave rise to distinct actin structures in swiss 3T3 fibroblasts (Nobes and Hall, 1995). While constitutively active RhoA led to the formation of bundles of actin stress fibers, constitutively active Rac1 and CDC42 formed protrusions containing thin sheet of branched actin filaments called lamellipodia and spike like structures of parallel actin bundles called filopodia respectively(Ridley and Hall, 1992; Ridley *et al.*, 1992; Nobes and Hall, 1995). Cell shape too is governed by the activities of Rho GTPases. Cells of different lineage display a variety of shapes, like columnar epithelial cells, stretched and branched neurons during morphogenesis, which are necessary for their functions(Jaffe and Hall, 2005; Paluch and Heisenberg, 2009). Remarkably, cells originating from a single population also exhibit different shapes, due to Rho GTPase

dynamics and their crosstalk involving their activation and mutual antagonism (Sailem *et al.*, 2014; Zmurchok and Holmes, 2020)

Cell migration is another complex process that is facilitated by the combined action and cross-talk of RhoA, Rac1 and CDC42. Rac1 is activated at the leading edge of a migrating cell to form lamellipodium. CDC42 determines the direction of migration (Raftopoulou and Hall, 2004). RhoA regulates focal adhesions assembly, stress fiber formation and activation of contractile myosin fibers. RhoA also severs the old focal adhesion contacts at the rear end of cell and its inhibition in migrating monocytes causes tail retraction defect and cell elongation (Worthylake *et al.*, 2001). Presented above is the simple model for cell migration, though evidence of cross talk between these GTPases is also known (Ridley *et al.*, 2003).

Activity of Rho GTPases is very tightly regulated, mainly by 3 kinds of proteins. Guanine nucleotide exchange factors (GEFs) activate Rho GTPases by catalysing the exchange of GTP to GDP bound Rho GTPase, GTPase activating proteins (GAPs) inactivate Rho GTPases by increasing their intrinsic GTPase activity, and Guanine nucleotide dissociation inhibitors (GDIs) interact with either GTP or GDP bound GTPases, masking their prenyl tails and sequestering them in the cytosol (Jung *et al.*, 2020). In absence of GDIs, Rho GTPases are targeted for proteasomal degradation (Boulter *et al.*, 2010). Apart from these, Rho GTPases are also regulated by various post-translational modifications which determine their sub-cellular localization, activity or stability (Hodge and Ridley, 2016; Navarro-Lérida, Sánchez-Álvarez and del Pozo, 2021). Due to the intricate spatio-temporal control of Rho GTPase activity and their crucial roles in key pathways, their dysregulation has been implicated in several cancers. (Pillé *et al.*, 2005; Cho *et al.*, 2018).

In eukaryotes, SET1 (KMT2) family proteins introduce the Histone 3 Lysine 4 (H3K4) tri, di- and mono-methylation marks (Zhang and Bergamin, 2012). Humans contain six members in this family including Mixed Lineage Leukemia protein (MLL) 1 to 4; SETD1A

and SETD1B. Out of these, the founding member —MLL1 (hereafter referred to as MLL) is the best characterized because of its role in aggressive leukemia (Patel *et al.*, 2009). MLL, a large nuclear protein, is processed post-translationally into MLL-N and MLL-C subunits(Hsieh *et al.*, 2003). MLL-N contains several chromatin binding domains while MLL-C provides catalytic Su(var)3–9, Enhancer-of-zeste, Trithorax (SET) domain and trans-activation domain (TAD) to activate transcription (Ernst *et al.*, 2001). As opposed to global activity of SETD1A, MLL methylates defined target genes(Wang *et al.*, 2009). Transcriptional maintenance of *HOX* genes by MLL in development of mammalian embryos is well documented. MLL is also required for hematopoesis and skeletal development (Cohn *et al.*, 1997; Hess *et al.*, 1997). MLL-null mouse do not survive beyond embryonic day 10.5 due to failure of continuous transcriptional maintenance of genes during development(Yu *et al.*, 1998).

Here we describe the role of MLL in the regulation of activity and stability of Rho GTPases—RhoA, Rac1 and CDC42. MLL depleted cells display atypical cell shape and loss of actin fibers resulting in defective cell spreading and migration. Stabilization of Rho GTPase levels depends on MLL's catalytic SET domain yet MLL does not affect their transcript levels. We show that MLL regulates the stability of Rho GTPases by transcriptional activation of RhoGDI1 using its methyltransferase activity. Using xenograft experiments, we show that targeting methyl transferase activity of MLL using small molecule inhibitor, OICR-9429. reduces size of tumors formed from triple-negative breast cancer (TNBCs) cell lines like MDA-MB-231. Our findings characterize MLL as the upstream regulator of RhoA, Rac1 and CDC42 GTPases, and identify MLL as a potential novel therapeutic target for triple-negative breast cancer.

Results

Loss of MLL causes changes in cell shape and actin cytoskeleton.

Mammalian cells attain various complex shapes. To understand the role of MLL in regulating cell shape, we performed RNAi experiments using specific MLL siRNA (Ali *et al*., 2014) and probed immunoblots with anti-MLL antibody (Figure 1A, S1A). The cells were subjected to indirect immunofluorescence staining (IF) using anti-α–tubulin antibodies. We observed that U-2OS cells depleted of MLL assumed an elongated shape compared with control siRNA-treated cells (Figure 1B). Ongoing studies from our laboratory indicate that MLL depletion does affect *de novo* microtubule polymerization from the microtubule organizing center (Chodisetty and Tyagi, unpublished). However, we could not detect any distinct microtubule organization in MLL siRNA-treated cells, except that they bunched together in elongated parts, probably due to cell shape (Figure 1B, see panel d-f). Besides microtubules, cell shape is also governed by the actin cytoskeleton and intermediate filaments (Luxenburg and Zaidel-Bar, 2019). Therefore, we stained the cells with rhodamine dye-conjugated-phalloidin, a peptide toxin known to bind filamentous actin (F-actin) with high affinity. Phalloidin-stained actin stress fibers could be clearly visualized in control cells (Figure 1C, panel a-c, a'-c', S1B). In contrast, in MLL-depleted cells, we observed a dramatic loss of visually discernible actin stress fibers as well as changes in cell shape (Figure 1C, S1C). Based on the previous screen (Pascual-Vargas *et al.*, 2017), we could make out the following prominent cell shapes in control siRNA-treated U-2OS cells: (i) fan, (ii) triangular, and (iii) circular shape (Figure 1C, S1B). When cells were clumped, without clear shape, we classified these as "compact". In contrast, MLL-depleted cells exhibited two or three prominent protrusions and were classified as 'spindly' (Figure 1C, panel d-e, d'-e', S1C panel a-b) or 'triangular' (Figure 1C, panel g-h, g'-h', S1C panel d-e) shape respectively. The triangular shape observed in MLL-depleted cells differed from control cells as they exhibited elongated protrusion on one side [with number of distinct filopodia (Figure 1C, panel g-h, g'-

h') or no filopodia (Figure S1C, panel d-e)]. Therefore, we made the distinction in two shapes by classifying them as triangular 'normal' (Figure 1C, panel a-b, S1B, panel d-e) or triangular 'abnormal' (Figure 1C, panel g-h, g'-h', S1C, panel d-e). Notably, when circular shape was observed in MLL-depleted cells, the diameter of the cell was much smaller (compare Figure S1B, panel g-h to S1C, panel g-h). To make sure that these observed cell shapes were not an artifact of siRNA used, we used two different, previously used MLL siRNAs (Ali *et al*., 2014). As shown, treatment with both MLL siRNAs yielded similar counts in cell shape (Figure 1D, S1D-I). We observed that, fan and triangular 'normal' shaped cells were significantly lower in MLL siRNA treated cells (Figure S1D-E) whereas spindly and triangular 'abnormal' shaped cells were significantly higher (Figure S1G-H). The number of cells with circular or compact shape had similar count in all samples (Figure S1F, I). Next, we tried to observe the corelation of cell shape to presence or absence of actin fibers. However, this analysis was not feasible as we did not have sufficient number of cells in one or other population to make a statistical comparison. Nonetheless, irrespective of their shape, across all cell shape categories, we observed substantial decrease in actin stress fibers in MLL siRNA-treated cells (Figure 1E). Taken together, our findings indicate that MLL affects actin stress fiber formation as well as cell shape.

Depletion of MLL alters cell-spreading and cell migration.

Extracellular matrix (ECM) composition influences the downstream actin cytoskeleton remodelling (Reymond *et al*., 2012). In fact, ECM component coated substrates like fibronectin are often used to mimic tissue environment characteristic of human cancer metastases (Reymond *et al*., 2012). Rho GTPases and actin cytoskeleton play a crucial role in cell spreading on ECM coated surfaces. Therefore, we tested if the ability of cells to spread on ECM coated surfaces is affected due to loss of MLL. Our results show that there was a

significant loss of area occupied by the spread cells upon MLL knockdown (Figure 2A-B). Interestingly we also observed that within 4 hours of spreading on fibronectin coated surface, MLL-depleted cells adopted an elongated shape (similar to that on uncoated glass). We quantified this by measuring circularity ($c = 4\pi A/P^2$, $c = 1$ for perfect circle, $c < 1$ for elongated objects) of cells and found a significant decrease in circularity upon loss of MLL (Figure 2C). We also measured the aspect ratio (ratio of major axis to minor axis, ar>1 for elongated objects) which showed a significant increase compared to control cells (Figure 2D). Taken together with data in Figure 1, all these observations point to a role of MLL in regulation of cell shape.

As the cell shape and actin cytoskeleton were dramatically perturbed upon knockdown of MLL, we suspected that loss of MLL would also affect cell migration. To test our hypothesis, we performed transwell migration assays. Upon knockdown using two MLL specific shRNAs (Figure 2E), but not control shRNA, we observed reduced cell migration in U-2OS cells (Figure 2F-G, S2A). We also tested cell migration upon MLL down regulation in epithelial, TNBC cell line—MDA-MB-231 (Figure 2H), and observed results similar to those obtained in the osteosarcoma epithelial cells (Figure 2G).

Thrombin not only activates RhoA, Rac1 and CDC42 ranging from a few seconds to several minutes(Azim *et al.*, 2000; van Nieuw Amerongen *et al.*, 2000) but also stimulates cell migration by different mechanisms (Radjabi *et al.*, 2008). Since MLL-depleted U-2OS cells showed reduced migration, we wanted to know if stimulation of these cells with thrombin over longer durations affects cell migration. We found a significant increase in cell migration in control cells upon thrombin treatment (Figure 2I, compare lane 1 to lane 3). However, this difference was not apparent in MLL-depleted cells (Figure 2I, compare lane 2 to lane 4) indicating that MLL-depleted cells are insensitive to stimulation by thrombin.

Taken together, our studies indicated that MLL knockdown perturbs the actin cytoskeleton, which was associated with changes in cell shape and reduced cell migration.

MLL /Rho GTPases depletion causes loss of actin dynamics and lamellipodia

Our observations of elongated cells with poor F-actin fibers and reduced cell migration are reminiscent of studies describing loss of RhoA family members (Vega *et al.*, 2011; Reymond *et al.*, 2012). Thus, to compare the changes in actin cytoskeleton and cell shape observed here, we performed experiments to knockdown RhoA, Rac1 and CDC42, three of the best characterised Rho GTPases involved in actin cytoskeleton remodelling (Etienne-Manneville and Hall, 2002), by using previously published siRNAs (Methods, Figure 3A-C). We observed elongated cells upon RhoA and CDC42 siRNA treatments, similar to MLL knockdown (Figure 3D, S2B, 1C). Although, cell elongation upon loss of Rac1 has been reported previously (Guo *et al.*, 2006), we did not observe this phenotype in our studies (Figure 3D, S2B). This can be due to the use of Rac1 knock out (KO) MEFs in the previous study, where the Rac1 expression is completely abolished, as opposed to siRNA treatment here (Figure 3B)(Guo *et al.*, 2006).

We observed a significant reduction in actin stress fibers upon depletion of Rho GTPases (Figure 3D-E). In contrast, control siRNA-treated cells displayed distinct numerable actin stress fibers. Although, Rac1 siRNA-treated cells exhibited few prominent actin stress fibers (Figure 3D, compare panel c Vs i), but when counted, the numbers were significantly less than control cells (Figure 3D-E). Loss of Rac1 leads to a dramatic decrease of the dorsal but not the ventral stress fibers (Kovac *et al.*, 2013). This explained the diminished number of stress fibers upon Rac1 depletion even if a few prominent stress fibers remained. MLL depletion caused similar reduction in actin stress

fibers to that seen individually with RhoA, Rac1 and CDC42 (Figure 3E, Nobes and Hall, 1995; Guo *et al.*, 2006; Vega *et al.*, 2011; Huang *et al.*, 2016). Thus, our results here indicated that MLL might regulate one, or possibly more Rho GTPases.

Since all three major Rho GTPases being studied here showed defects in actin cytoskeleton assembly, we decided to use this assay to determine which domain of MLL is involved in this process. As transcription is the major activity ascribed to this protein, we focused on the 9 amino acid TAD, which promotes cooperative binding of coactivators to augment synergistic gene activation (Ernst *et al.*, 2001) and SET domain, which is required for its H3K4 histone methyltransferase activity (Figure S2C). We made use of previously described U-2OS cells stably expressing various FLAG-epitope tagged mutants of MLL (Figure S2C-D) *(*Ali *et al*., 2014, Malik *et al*., 2022 for TAD cell line). Depletion of endogenous MLL in these cell lines was achieved by use of siRNA targeting the 3' UTR of MLL transcript (siRNA#2, Figure 1A), wherein recombinant MLL expression is unaffected. Consistent with previous experiments, the number of actin stress fibers showed a reduction in wild type U-2OS cells upon treatment with MLL siRNA#2 (compare Figure 3F with 1E). When expression of MLL protein was reconstituted, actin stress fibers were rescued but not at the same levels as wild type U-2OS cells (Figure 3F). However, no further change was observed in stress fiber numbers once cells were treated with siRNA#2, indicating that actin stress fibers reduction could be specifically assigned to MLL . Out of the two transcription-promoting domains of MLL, absence of SET domain, but not TAD resulted in reduction of actin stress fibers, suggesting that the methylation activity of MLL promoted actin stress fiber formation (Figure 3F).

As the actin cytoskeleton diminished with the loss of MLL, we wanted to explore if actin dynamics in the cells were also affected. The primary driving force behind the motility and shape changes in cells depends on the dynamics of actin, which can be polymerised into

different networks and structures, and rapidly depolymerised (Blanchoin *et al.*, 2014). For studying the actin dynamics in real time, we made use of GFP-Lifeact, which binds to filamentous actin in live cells (Riedl *et al.*, 2008). U-2OS cells expressing GFP-Lifeact displayed well-formed lamellipodia, with rapid spreading and ruffling (Figure 3G, Movie 1 and 2) but were absent in MLL-depleted cells (Figure 3G, Movie 3 and 4). In fact, the actin dynamics in MLL siRNA-treated cells almost came to a halt. Consistent with our previous observations, MLL-depleted cells were elongated and exhibited numerous filopodia along the length of the cells (Figure 3G). The particle velocity estimated by generating kymographs (Figure 3G right panels) from the live cell movies, showed that the average track velocities reduced drastically in MLL-depleted cells (Figure S2E). These experiments confirmed the role of MLL in regulating actin dynamics in the cell.

Rac1 is a key regulator of lamellipodium extension (Ridley *et al.*, 1992). Our RhoA and CDC42-depleted cells displayed cell shapes similar to MLL depletion but Rac1-depleted cells had different cell shapes. Thus, to ascertain that MLL influenced Rac1 functions, we checked for lamellipodia formation in MLL depleted cells (Figure 3H). We used Nck-associated protein 1(Nap1), a part of WAVE regulatory complex, as a marker for lamellipodia. Nap1 migrates to the tips of membrane protrusions like lamellipodia upon Rac1 activation (Steffen *et al.*, 2004). We could observe a prominent lamellipodia in control-siRNA-treated cells, which displayed Nap1 enriched at its tip (Figure 3H). Whereas, fewer MLL-siRNA-treated cells formed lamellipodia, and membrane protrusions which formed, did not show Nap1 staining at the tips (Figure 3H-I). We further assessed if MLL SET domain was also involved in regulation of Rac1 function. Indeed, full-length MLL protein, but not the SET-domain deleted mutant, rescued lamellipodia formation (Figure 3I). Similarly, cell migration was also compromised for cells expressing SET-domain deleted mutant of MLL

(Figure S2F) indicating that MLL regulated the various functions of Rho GTPases by its histone methyltransferase activity.

RhoA, Rac1 and CDC42 are essential for cell spreading on fibronectin in different cell types (Reymond *et al*., 2012; Yang *et al.*, 2020). Since we found defects in fibronectin spreading upon of MLL depletion, we wanted to study if similar spreading defects were observed upon Rho GTPases knockdown. Consistent with previous reports, depletion of Rho GTPases led to significant impairment in cell spreading on fibronectin coated surface (S3A-B) but we did not observe any significant change in aspect ratio and circularity of cells (cell shape; S3C-D) as was observed upon MLL depletion (Figure 2C-D). These results indicate that similar to MLL, the Rho GTPases-depleted cells are slow to spread on fibronectin-coated surface but do not show cell elongation in the observed time. It is possible that upon MLL depletion, we may be observing the collective effects on more than one Rho GTPases which lead to a more severe cell shape phenotype than individual Rho GTPase depletion.

Loss of MLL leads to reduction of Rho GTPases protein stability and activity.

Our actin stress fiber, lamellipodia and cell migration assays indicate that MLL might regulate the three Rho GTPases. To find out how MLL may confer this regulation we decided to check for cellular levels of these GTPases upon MLL depletion. MLL knockdown resulted in a dramatic loss of total endogenous protein levels of RhoA, Rac1 and CDC42, quantified over multiple experiments in U-2OS cells (Figure 4A). We made similar observations in MDA-MB-231 cells (Figure S4A). To check if this reduction in total protein translated to loss of activity of these Rho GTPases, we tested for active GTPases in our system.

Classical Rho GTPases like RhoA, Rac1 and CDC42 act like molecular switches. To study their activities we used previously established assays utilizing their binding to effector domains (Ota *et al.*, 2007; Ito*et al*., 2018). Due to technical difficulties in detecting

endogenous Rho proteins in above assay, we expressed all three RhoA, Rac1 and CDC42 as green fluorescent protein (GFP) fusion proteins. Anti-GFP antibody was used to detect all three GTPases, which also removed the impact of specific antibodies on our assay. Upon MLL depletion, we saw a striking loss of active and total protein of RhoA, Rac1 and CDC42 (Figure 4B-C). Our results imply that MLL-depleted cells undergo a decrease in total protein levels of Rho GTPases which manifest itself eventually in the active protein levels, finally leaving the cell with very little active Rho GTPases pool.

As MLL is an established transcription co-activator; we thought MLL might be transcriptionally regulating the Rho GTPases expression. Therefore, we checked the transcript levels of *RHOA*, *RAC1* and *CDC42* after MLL depletion. Although *MLL* mRNA levels were reduced by 70-75% in our experiment, we did not find any significant change in expression of *RHOA* and *CDC42* upon MLL depletion (Figure 4D). Even though relative expression of *RAC1* reduced upon MLL knockdown, it was not enough to cause near complete reduction of protein levels as seen in Figure 4A. Our results thus far indicate that MLL regulates the protein levels but not the transcript levels of Rho GTPases.

Down regulation of MLL affects the protein and transcript levels of RhoGDI1.

Unchanged RhoA, Rac1 and CDC42 transcript levels upon MLL knockdown prompted us to search for a causal factor that affects the stability of all three Rho GTPases. Literature search revealed that depletion of RhoGDI1 affected the protein levels of major Rho GTPases including the ones being studied here (Boulter *et al.*, 2010). To ascertain if MLL knockdown affects RhoGDI1, we checked the RhoGDI1 protein levels in control and MLL-depleted cells. As shown in Figure 5A, the levels of RhoGDI1 were considerably reduced upon MLL knockdown. We also used CRISPR-Cas9 system to generate inducible MLL knockout (iKO) HEK-293 cell lines (Figure S4B). RhoGDI1 protein levels were significantly

reduced in two independent MLL iKO clones (Figure 5B, S4C). Finally, we tested our hypothesis by performing a dose-dependent depletion of MLL. Upon transfecting increasing amount of MLL shRNA#2 plasmid, we observed gradation in decrease of MLL protein levels (Figure S4D, panel a). These changes were accompanied by corresponding gradation in decrease in RhoGDI1 protein levels as well as those of RhoA, Rac1 and CDC42 (Figure S4D), indicating that MLL regulated RhoGDI1 protein levels to regulate these RhoGTPases.

To determine if RhoGDI1 is a transcriptional target of MLL, we measured it's transcript levels in MLL siRNA-treated cells. The *MLL* levels were reduced by more than 60% and we observed a corresponding decrease in the *RHOGDI1* transcript (Figure 5C). Even though RhoGDI1 is the most abundant and ubiquitously expressed member of the GDI family, we also tested transcript levels of *RHOGDI2* and *RHOGDI3*, primarily expressed in haematopoietic cells and brain respectively (Gorvel *et al.*, 1998). These transcripts showed no significant change upon loss of MLL (Figure 5C) indicating that MLL specifically regulated RhoGDI1 in these cells. Next, we asked if like all the Rho GTPases-regulated phenotypes studied above, the MLL-mediated regulation of *RHOGDI1* transcript was also SET domain-dependent. Indeed, expression analysis of *RHOGDI1* indicated that its levels were restored in presence of MLL full-length protein but decreased in the absence of SET domain-deleted MLL mutant (Figure 5D). Based on our results so far, it seems likely that RhoGDI1 may be the common denominator in regulation of Rho GTPases by MLL.

Up to 95% of cellular levels of RhoA, Rac1 and CDC42 are maintained by RhoGDI (Boulter *et al.*, 2010). We confirmed these findings by generating stable KOs of RhoGDI1 in U-2OS cells by genome editing. We used two individual clones for our experiment, where both the clones showed complete KO of RhoGDI1 (Figure 5E, S4F). As expected, the protein levels of RhoA, Rac1 and CDC42 were highly diminished in these cell lines (Figure S4E, G), indicating that RhoGDI1 indeed regulated majority of Rho GTPases protein levels. We also

compared the number of stress fibers in control and RhoGDI1 (KO#1) cells. Consistent with the absence of the three GTPases, we found that the number of stress fibers was drastically reduced in both RhoGDI1 KO cells (Figure 5F-G). Previous reports indicated that loss of RhoGDI1 is associated with a mild phenotype (Boulter *et al.*, 2010). As these studies were based on the siRNA knockdown of RhoGDI1, we depleted RhoGDI1 using siRNA (Figure S5A). RhoGDI1-depleted cells displayed very little actin stress fibers, similar to the RhoGDI1 KO cells (compare Figure 5F-G to S5B-C) and there was significant reduction in area of spread of these cells (Figure S5D-E). We found no change in circularity and aspect ratio of cells (Figure S5F-G) similar to Rho GTPases knockdown. In contrast, RhoGDI1 KO cells showed significant spreading defects (Figure 5H) as well as significant increase in circularity and hence reduction in the aspect ratio (Figure 5I-J). Our results indicate that transient knockdown as well as stable knockout of RhoGDI1 have similar effects on stress fiber formation and cell spreading as does MLL loss (compare 1E, 5G and S5C; 2B, 4H and S5E). However, transient RhoGDI1 depletion but not the knockouts, have a more severe effect on cell shape similar to MLL depletion (compare Figure S5B, 5F and 1C). Taken together, our results show that MLL modulates the protein levels of RhoA, Rac1 and CDC42 by regulating the transcript level of RhoGDI1 .

MLL binds to RhoGDI1 promoter to bring about H3K4 trimethylation.

Based on our results, we propose that RhoGDI1 may be a transcriptional target of MLL. To determine if this regulation is direct, we performed chromatin immunoprecipitation (ChIP) experiments and analysed for MLL binding on RhoGDI promoters. Our transcript data showed that MLL only affected the transcript levels of RhoGDI1 and not RhoGDI2 or RhoGDI3 (Figure 5C). To confirm these observations, based on the RNA polymerase II enrichment in UCSC genome browser (Barski *et al.*, 2007), we chose the upstream and

promoter region of all three RhoGDIs as shown (Figure 6A). We selected a well-characterized MLL target —*HOXA9*, for positive control and *CD4*, a gene that is not expressed in chosen cells for negative control. IgG was used as antibody control. We performed the ChIP experiments in both transformed (HEK-293T) as well as non-transformed (IMR-90tert) cell lines. ChIP-PCR analyses in these two cell lines indicated that, consistent with our transcript data, MLL showed significant enrichment only on RhoGDI1 promoter but not RhoGDI2 and RhoGDI3 (Figure 6B-C, S6A). This enrichment of MLL correlated with the presence of H3K4me2 and H3K4me3 marks at RhoGDI1 promoter (Figure 6D-E, S6B-C). Curiously, we observed presence of H3K4me2 marks on RhoGDI3 promoter in both the cell lines (Figure S5B-C). However, these were not accompanied by the H3K4me3 marks suggesting that these promoters may not be actively transcribed in these cell lines.

Our data, so far, indicate that MLL regulates RhoGDI1 transcription by its histone methyltransferase activity. To confirm our hypothesis, we used our MLL-iKO cells to perform ChIP experiments. The MLL levels were severely reduced in iKO cells when compared to the control cells (Figure 6F). Consistent with our hypothesis, the H3K4me3 and H3K4me2 marks were correspondingly reduced on the RhoGDI1 promoter (Figure 6G, S6D). Thus, our results indicate that MLL specifically regulates RhoGDI1 by methylating its promoter and activating transcription.

Exogenous expression of RhoGDI1 can rescue some phenotype associated with loss of MLL

MLL is a transcriptional regulator for hundreds of genes (Wang *et al.*, 2009). However, our findings indicate that the phenotypes related to cell shape and migration being studied here may be due to the loss of major Rho GTPases, which are in turn governed by the

transcript/protein levels of RhoGDI1. Therefore, we wanted to test whether restoration of RhoGDI1 protein levels in MLL-depleted cells would rescue Rho GTPase protein levels, cell shape, migration and actin stress fiber formation defects. To answer these questions, we expressed RhoGDI1 conditionally upon drug induction. We could clearly detect RhoGDI1-GFP upon induction with Doxycycline (Figure S7A), which was absent in the uninduced control cells. We then transfected these cells with control and MLL siRNA, and probed for RhoGDI1-GFP as well as endogenous RhoGDI1 (Figure 7A). While the endogenous RhoGDI1 protein levels diminished substantially in MLL-depleted cell, the exogenous RhoGDI1-GFP expression was unaffected (Figure 7A, compare panel c with d). In line with our hypothesis, we next checked for protein levels of RhoA, Rac1 and CDC42 in RhoGDI1-GFP cell line in control- and MLL-siRNA-treated cells. We observed that exogenous expression of RhoGDI1-GFP was able to restore the endogenous expression of RhoA, Rac1 and CDC42 proteins despite MLL siRNA treatment, comparable to control cells (Figure 7A). These results indicate that RhoGDI1 was indeed the major factor responsible for regulating RhoA, Rac1 and CDC42 protein levels upon loss of MLL. Given that the major Rho GTPases levels were restored in the cell, we performed cell migration assays in RhoGDI1-GFP expressing cells using control and MLL shRNA. As reported before, we observed reduced cell migration upon MLL shRNA treatment (Figure 7B-C, 2G-H) in U-2OS cells. Surprisingly, control shRNA-treated cells, expressing RhoGDI1-GFP, also showed reduced cell migration when compared to U-2OS cells (control). This was probably the indirect consequence of sequestering active Rho GTPases by overexpressed RhoGDI1(Golding *et al.*, 2019). However, when MLL was depleted using shRNA in these cells, the cell migrated faster (Figure 7B-C). Even though the cell migration was not restored to level of wild type cells, our results suggest that RhoGDI1 is a key factor affecting cell migration upon MLL-depletion.

Mis-regulated expression of RhoGDI1 is associated with many different cancers. Notably, upregulated expression of RhoGDI1 in certain cancers is associated with enhanced invasion, metastasis, and chemoresistance (Fritz *et al*., 1999; Hondermarck *et al.*, 2001; Zhang *et al.*, 2005). We noted that MDA-MB-231 cells exhibit high expression of RhoGDI1 (Figure S7B). The MDA-MB-231 cell line is commonly used to model, late-stage triple-negative breast cancer (Betapudi *et al*., 2006). To assess if our findings here can have clinical relevance, we used a small molecule inhibitor, OICR-9429, which binds specifically to WDR5 and inhibits its interaction with MLL, thereby the methyltransferase activity of MLL complex (Grebien *et al.*, 2015) for the treatment of these TNBC cells. Treating MDA-MB-231 cells with 25μM OICR-9429 for 72 hours significantly reduced the expression of RhoGDI1 transcript (Figure 7D). Similar to MLL RNAi treatment, OICR-9429 treatment also resulted in fewer migrating cells when compared to the control in transwell migration assay (Figure 7E). To investigate the efficacy of OICR-9429/depletion of MLL on TNBC *in vivo*, we performed xenograft assays in nude mice. MDA-MB-231 cells were treated with either MLL or RhoGDI1 shRNA and engrafted in breasts of female nude mice by subcutaneous injection. MLL or RhoGDI1 shRNA treated cells showed substantially small tumor size compared to control set (Figure 7F, S7C). Similarly, in mice engrafted with MDA-MB-231 cells, intravenous injections with 4 mg/Kg OICR-9429, showed a significant reduction in size of tumors as compared to those injected with vehicle (Figure 7G). Taken together, our results identify MLL as a potential new target to treat TNBC (or any other cancers) with upregulated expression of RhoGDI.

Discussion

MLL regulates cell shape, actin cytoskeleton and cell motility.

Here we report the role of MLL in regulating cell-shape and migration as a consequence of regulating actin cytoskeleton via stabilizing Rho GTPases. MLL or its complex proteins like WDR5 and Dpy30 have been deemed important for cell migration (Wang *et al.*, 2018; Malek *et al.*, 2017; He *et al.*, 2019; Zhang *et al.*, 2020; Artinger *et al.*, 2013). Similarly, different family members like MLL2 and MLL3, through different targets and modes, affect cancer cell motility and survival (Xia *et al.*, 2015; Issaeva *et al.*, 2007). Rho GTPase signalling is central to the formation and maintenance of actin cytoskeleton. In MLL-rearranged leukemia, at least 18 fusion partners are involved in Rho GTPases signalling (Marschalek, 2016). Many of them are GEFs and GAPs, highlighting the importance of cross talk of Rho GTPases signalling, and MLL in cancer. Possibly, MLL's fusion with such proteins might give the leukemic cells a selective advantage in anchorage and metastasis by altered actin dynamics. In support of this hypothesis, knocking down MLL-AF6 fusion led to dramatic changes in cell shape and actin cytoskeleton in SHI1 (human AML cell line) cells (Tregnago *et al.*, 2020). We observe similar cell shape phenotypes upon loss of MLL and three Rho GTPases suggesting that MLL regulates these Rho GTPases directly or indirectly.

MLL is responsible for the homeostasis of Rho GTPases by transcriptional activation of RhoGDI1

Our study revealed the role of MLL in stabilization of endogenous as well as over-expressed RhoA, Rac1 and CDC42 proteins. We performed our activity assays with over-expressed Rho GTPases, which is not a norm but has been reported (Shi et al., 2017; Zhou et al.,

2010). However, the stoichiometry and equilibrium of RhoGDI-bound Rho proteins change with the over-expression of any one Rho GTPases (Boulter *et al.*, 2010). Nonetheless, our assays showed reduced Rho GTPase activity upon MLL knock-down which was consistent with our other observations showing defects in actin cytoskeleton, lamellipodia formation, reduced actin dynamics and cell spreading following MLL loss. Remarkably, all three Rho GTPases proteins studied here are at the epicenter of extensive signalling pathways. Regulatory proteins which can modulate their active/total protein levels can influence various cellular processes. In agreement with this, over-expression of human MLL in murine c-Kit+/Cd41+ embryonic stem cells increases the cells with multi-lineage differentiation capacity by stimulating Rac/ Rho/ integrin signalling pathways rather than conventional MLL targets like *HOX* genes (Yang *et al.*, 2020). Thus, this study underscores the wider influence of MLL on cellular pathways controlled by Rho GTPase signalling.

Rho GTPases are stabilized by three RhoGDIs. RhoGDI1 is ubiquitously expressed, and its knockdown leads to reduced protein stability of RhoA, Rac1 and CDC42 (Boulter *et al.*, 2010). Our experiments show that RhoGDI1 levels are transcriptionally regulated by MLL-mediated H3K4 trimethylation. Besides protein levels, how the activity of RhoGDI1 is regulated, still needs to be unravelled. For example, how certain cancers sustain high RhoDI1 expression is still unknown. Over-expression of RhoGDI1 is toxic for certain cell types (Miura *et al.*, 1993, this study). On the other hand, RhoGDI1 is highly expressed in many cancers, conferring tumour cells with high metastatic and invasive potential, and drug resistance(Fritz *et al*, 1999; Hondermarck *et al.*, 2001; Zhang *et al.*, 2005). Even though protein levels of RhoA, Rac1 and CDC42 were rescued after induced over-expression of RhoGDI1, the stress fibers were not replenished. On the contrary, consistent with previous findings, we found defective actin polymerisation and shape in cells expressing GFP-RhoGDI1 (unpublished data; Miura *et al.*, 1993). It is likely that RhoGDI over-expression

stabilized the overall Rho GTPase protein levels but extracted the active forms from the membrane (Golding *et al*., 2019). Similarly, cells expressing MLL full-length protein showed reduced actin stress fibers cell migration (Figure 3F,S2F) compared to U-2OS cells. Even though, these effects were not as drastic as RhoGDI1 expression (compare Figure S2F to Figure 7C), we speculate that these may be a consequence of increase in RhoGDI1 expression upon MLL ectopic expression. Supporting our hypothesis, previous studies show that RhoGDI1 over-expression causes migration defects (Yu *et al.*, 2012). Collectively, these observations imply that appropriate expression of RhoGDI1 in cells is of utmost importance and any variation may lead to undesirable consequences.

MLL depletion causes reduction of size of xenografts.

TNBCs, which account for 15% of total breast cancer cases, are characterised with high proliferative rate, greater brain metastases, early onset and poor prognosis (Dangi and Firodiya, 2012). Here, the tumour cells do not express receptors for estrogen, progesterone or ERBB2 protein, making them resistant to conventional hormone treatment regime with no definite treatment available. MDA-MB-231 is one such TNBC-derived cell line with high RhoGDI1expression and a model for studying breast cancer *in vivo*. We show that MLL and RhoGDI1 depletion in MDA-MB-231 produce smaller tumors in nude mice. Although, MLL fusion proteins vastly deregulate the gene expression profile of the transformed cells, sustenance of leukemogenesis in these cells still requires one functional allele of MLL. Thus, targeting MLL's catalytic activity with small molecule inhibitors has yielded considerable success in treating cancer in mouse models(Ye *et al.*, 2019; Thiel *et al.*, 2010; Ansari *et al*, 2013). We chose a non-peptide inhibitor of MLL-WDR5 interaction, OICR-9429, which was already reported in treating various cancers in mouse models (Grebien *et al.*, 2015; Carugo *et al.*, 2016). With OICR-9429 treatment in MDA-MB-231 cells, we report significant reduction

of gene expression of RhoGDI1translating into reduced size of xenografts formed from these cells in nude mice. Taken together our results indicate a new target for treatment of TNBC using small molecule inhibitor affecting catalytic activity of MLL. We believe similar approach can be utilised for treating other cancers showing over-expression of Rho GTPases and RhoGDI.

Methods

Cloning

Complementary DNA (cDNA) encoding RhoA, Rac1, CDC42 and RhoGDI1 were amplified from cDNA generated from human osteosarcoma (U-2OS) cell line using Phusion polymerase (NEB, M0530). These cDNAs were cloned in Xho I linearized pCDNA vector with GFP in the N terminus yielding GFP- RhoA/Rac1/CDC42/RhoGDI1 constructs. For ectopic inducible expression of RhoGDI1 in U-2OS cells, we deleted the Cas9 gene from the pCW Cas9 vector, gift from Eric Lander & David Sabatini (Wang *et al.*, 2014), and incorporated EcoR1 site at its place by inverse PCR. GFP-RhoGDI1 (PCR-amplified from pCDNA GFP-RhoGDI1 described above) was then cloned in the EcoR1 sites using In-Fusion® HD Cloning Kit (Takara, 639649). RhoGDI1 sgRNA1 (CAGGCCAGTCACCACGACGT) and sgRNA2 (CCCCAACGTCCCCAACGTCG) were cloned in LentiCRISPRv2, a gift from Brett Stringer (Stringer *et al.*, 2019) in BsmB1 sites. MLL sgRNA1 (CGAACATGGCGCACAGCTGT) and MLL sgRNA2 (CAGCGGGGCTGGGGTTCCAG) were cloned into Lentiguide-puro vector, gift from Feng Zhang (Sanjana *et al.*, 2014) in BsmB1 site. RhoGDI1 shDNA1(CGTCTAACCATGATGCCTTAA), RhoGDI1 shDNA2 (TCCGGGTTAACCGAGAGATAG), MLL shDNA1 (CTACCAACCCTAAACCCTG), MLL shDNA2 (GCCTCCATCAACAGAAAGGAT), and control shDNA

(GCGCGATAGCGCTAATAATTT), were cloned in PLKO.1 vector in Kpn1 and EcoR1 sites. All constructs were verified by sequencing. GST-tagged Rho Binding Domain of Rhotekin (RBD) and p21 Binding Domain (PBD) of p21 activated kinase1 protein for pull downs of GTP bound RhoA and CDC42/Rac1 respectively were kind gifted by Dr. Keith Burridge. p^{CMV}-LifeAct-TagGFP2 (Ibidi, 60101) vector was a gift from Dr. Rashna Bhandari.

Cell culture, transfection and stable cell-line generation

All cell lines were authenticated by STR profiling and checked for contamination. A549 was a gift from Dr. A. Ramteke, Tezpur University. Cells were grown in Dulbecco's modified Eagle's medium supplemented with 10% fetal bovine serum, L-glutamine and penicillin/streptomycin. U-2OS cells stably expressing GFP-tagged RhoA, Rac1, CDC42, and RhoGDI1 were obtained by transfecting cells with Polyethylene imine (PEI; Polysciences 23966-2). MDA-MB-231 cells expressing control, MLL and RhoGDI1 shRNA were obtained by lentiviral transduction as described before (Van Lidth de Jeude *et al.*, 2015). The transduced and transfected cells were selected using 4µg/ml and maintained using 2µg/ml Puromycin (Gibco 11138-03). Drug-resistant colonies were tested for recombinant gene expression by immunoblots. Two different RhoGDI1 sgRNAs were transfected in U-2OS. Serial dilution was done to obtain single cell colonies after Puromycin (4µg/ml) treatment. Colonies were screened for RhoGDI1 KO by Western blot .

For our experiments, we generated inducible MLL knock-out in HEK293 cells. To achieve this Doxycycline-inducible Cas9 expression vectors (pCW-Cas9), was modified by replacing the Puromycin resistance gene with Blasticidin. pCW-Cas9-Blast vector was packaged as lentivirus and HEK293 cells were transduced with these viral particles. Cas9 positive colonies were selected with 5µg/ml Blasticidin (Invitrogen R21001). Once single colonies were selected by screening for Cas9 expression (upon induction with Doxycycline 2µg/ml;

Sigma D9891) by Western blot, these colonies were transduced with both MLL sgRNA (described above) viral particles. Cells were selected with Puromycin (2µg/ml). Single colonies were screened for loss of MLL expression by Western blot, and two clones were selected for further analysis (#11 and #20). MLL knockout was initiated by inducing cells with 4µg/ml of Doxycycline for seven days. MLL knockout was confirmed with Western blot, before proceeding for ChIP experiments.

For making GFP-RhoGDI1 cell lines, after transfection, U-2OS cells were selected by 4µg/ml Puromycin. Single cell derived colonies were induced with 2 µg/ml Doxycycline and screened for RhoGDI1 expression by performing Western blot.

siRNA and shRNA transfections

siRNA transfections were performed as described earlier (Tyagi and Herr, 2009). Cells were harvested 72 hr. after first transfection and either used for RNA extraction, or fixed for immunofluorescence studies or lysed in sodium dodecyl sulphate Laemmli buffer and subjected to Western blotting. Control siRNA (CGUCGCGGAAUACUUCGA), MLL siRNA#1 (AAGGAAAGCAUUACUGAGAAAUU) and MLL siRNA#2 (ACGAAAGACTGAATGTAAAUU) were purchased from GE Dharmacon as described before (Ali *et al.*, 2014). Previously described siRNAs against RhoA (GAACUAUGUGGCAGAUAUCUU), Rac1 (CGGCACCAUGUCCCAACAUU), CDC42 (GGAGAACCAUAUACUCUUGUU) and RhoGDI1 (UCAAUCUUGACGCCUUUCCUU) were purchased from Sigma (Boulter *et al.*, 2010; Reymond *et al.*, 2012). shRNA described above were transfected using PEI in U-2OS. For transwell migration assay, cells were subjected to one round of shRNA transfection. For pulling down active forms of Rho GTPases, cells were subjected to 2 rounds of shRNA transfection at 24 hours interval. For dose dependent MLL knockdown, U-2OS cells in 10 cm plates were treated with 10µg (one

round of transfection), 20 µg (2 rounds of 10µg DNA transfections, 24 hours apart) or 30 µg (3 rounds of 10µg DNA transfections, 24 hours apart) of control (scrambled) or MLL shDNA and incubated for 72 hr. Post incubation, cells were harvested, lysed and immunoblotted.

RNA isolation and quantitative real-time polymerase chain reaction

RNA was extracted either by Trizol (Ambion 15596018) extraction method or Directzol RNA Miniprep kit (Zymo Research R 2050). Two micrograms of the total RNA was used to prepare cDNA using Superscript III reverse transcriptase (Invitrogen 1808005) and cDNA was used for real-time quantitative polymerase chain reaction (RT-qPCR) using SYBR green kit (ThermoFisher, F416L). Each sample was run in triplicate. The amplification was performed and detected using 7500 Real Time PCR system (Applied Biosystems). Transcripts were normalized to the housekeeping gene GAPDH by using −ΔΔCT method for determining relative gene expression (Livak and Schmittgen, 2001). Primers used for PCR amplifications are described in supplementary data Table 1.

Protein pull-downs

Lystaes of GFP tagged RhoA and Rac1 or CDC42 expressing cells, treated with control or MLL shRNA, were prepared by lysing cells in NETN buffer (100mM NaCl, 20mM Tris pH 8, 0.5mM EDTA and 0.5% Nonidet p 40) in presence of protease inhibitors, and PMSF, and incubated with Glutathione S Transferase (GST) tagged RBD and PBD immobilized on glutathione beads (Sigma G4510) respectively, for 2 hours at 4^0C. The beads were washed with wash buffer (50mM Tris pH 7.4, 100mM KCl, and 0.05% Nonidet p 40) and used for immunoblot analysis.

Immunoblots

Immunoblotting was done onto nitrocellulose (Amersham 10600003) or PVDF (Amersham 10600023) membrane. Transfer was done using Tris-Glycine Transfer buffer containing 10% Methanol for 2 hours at 225 mA. Blots were blocked using 5% skimmed milk in PBS-T and then probed with either of the following primary antibodies overnight at 4^0C: RhoA (St. John's Laboratories 95442) (1:100), CDC42 (St. John's Laboratories 191678) (1:100) , Rac1 (Abcam 33186) (1:5000), GAPDH (Cloud Clone Corp. PAB932Hu01) (1:5000), Tubulin (Sigma T5168) (1:10000) antibody, RhoGDI1 (St. John's Laboratories 22675)(1:5000). For imaging in Licor imaging system, following fluorescently labelled secondary antibodies were used at 1: 10,000 dilution: Goat anti mouse IR dye 800 CW (Li-cor 926-33210), Goat anti rabbit IR dye 800 CW (Li-cor 926-32211), Goat anti mouse IR dye 680 CW (Li-cor 926-68020), Goat anti rabbit IR dye 680 CW (Li-cor 926-68021). For imaging in a chemiluminiscence system, Horse Radish Peroxidase (HRP) conjugated secondary antibodies raised either in mouse (Bio-Rad, 170-6516) or rabbit (Bio-Rad, 170-6515) were used at at 1: 10000 dilution. Please see Figure S8 for whole blots used in the figures.

Generation of MLL_C antibody

GST-tagged fragment of MLL_C containing amino acids (2700-3092) named as MLL D1 was utilised for antibody generation. Protein was produced as described in (Ali *et al.*, 2017). GST–MLL D1 was eluted in elution buffer {Tris-Cl (50 mM, pH=8.8), 30 mM reduced glutathione (Sigma G4251)} for 2 hours at 4^0C. Elute was dialysed over night at 4^0C in dialysis buffer (120mM NaCl, 2mM $MgCl_2$,10% glycerol, 20mM HEPES pH 7.9). Antibody was generated in rabbit at Bioklone Biotech Private Limited, Chennai, India. Subsequently, specificity of antibody was checked by performing MLL specific siRNA/shRNA by Western blots (see Figure 1A, 2E, S1A).

Immunofluorescence

Unless being used for fibronectin spreading assay, cells were grown on cover slips for immuno fluorescence experiments. After appropriate treatment, cells were fixed with either 4% paraformaldehyde (Sigma 158127) solution prepared in Phosphate buffered saline (PBS) at room temperature for 10 minutes for rhodamine conjugated phalloidin (ThermoFisher Scientific R415) staining or with 10% trichloroacetic acid (Amresco 133) at 4^0C for 10 minutes for Nap1 antibody (St. John's Laboratories 114120) staining. Permiabilization of cells prior to phalloidin/antibody staining was done using 0.2% Triton X100 (Amresco 0694). The cells were then incubated with phalloidin or NAP1 antibody for 1 hour at room temperature. When staining for NAP1, anti-rabbit Alexa fluor 488 secondary antibody (Invitrogen A 11034) was used. The cover-slips were then washed with a solution of 4',6-diamidino-2-phenylindole (DAPI; Sigma D9542), mounted on slides and visualized under Zeiss LSM 700 Confocal microscope or Leica SP8 confocal microscope.

For quantification of stress fibers, images were opened in image J and number of stress fibers were counted manually by using multipoint selection tool. Number of cells that were used to calculate stress fibers were also noted. Number of stress fibers per cell was expressed as a ratio of sum of all the stress fibers obtained in the experiment to the number of cells imaged. Presence or absence of lamellipodia in the cells was determined visually by the presence or absence of membrane staining of Nap1 in cells. The results were plotted by describing the number of cells with and without lamellipoida.

For time-lapse imaging, U-2OS cells expressing p^{CMV}-LifeAct-TagGFP2 vector were seeded on a glass bottom dish. siRNA transfections were carried out as discussed above. After incubation, cells were imaged in Zeiss Elyra 7 microscope in Lattice SIM mode at 5 seconds interval for 2 minutes and 25 seconds. Kymographs of these images were generated using a Fiji script (tsp050706.txt Kymograph {TimeSpacePlot} by Jens Rietdorf, available at

http://www.embl.de/eamnet/html/kymograph.html). Analysis of kymographs was done as described previously (Jakobs *et al*., 2019). Average track velocities thus generated were plotted as scattered plot using GraphPad prism and significance analysis was performed.

Cell spreading Assay

For coating, coverslips were incubated with 200 µg/ml fibronectin (Sigma F2006) dissolved in PBS and coated on coverslips for 30-45 minutes at room temperature in aseptic conditions. The solution was removed and coverslips were rinsed with DMEM or PBS. For fibronectin spreading assay, cells were directly seeded in 6 well plates and after completion of siRNA treatment (72 hrs), cells were trypsinised and 10^5cells were reseeded on fibronectin coated coverslips for 4 hours before fixing for immunofluorescence. For quantifications of area of spread, circularity and aspect ratio, images were opened in image J. Edges of the cells were marked using free hand selection tool. 'Shape Descriptor' plug-in was used to calculate, area of spread, circularity and aspect ratio of that particular ROI. The data thus obtained was saved in Excel files and used for plotting graphs in GraphPad Prism.

Transwell Migration Assay

U-2OS/MDA-MB-231 cells, after MLL shRNA/OICR-9429 treatment, were trypsinised and counted using hemocytometer. For thrombin treatment, U-2OS cells treated with control or MLL shRNA were incubated in DMEM containing 4U/ ml thrombin (Sigma, T4648) for 48 hr. For OICR-9429 treatment, MDA-MB-231 cells seeded in 6 well plates were treated with 25 µM OICR-9429 for 72 hours. Control cells in same experiments were treated with DMSO. U-2OS GFP-RhoGDI1 cells were additionally treated with 2 µg/ml Doxycycline. 10^5 cells from the above-mentioned treatments were suspended in 200 µl of DMEM containing 1% FBS. The cell suspension was carefully added to the cell culture inserts (BD falcon 353097).

These inserts were immediately put in the wells of 24 well plate containing complete media and incubated for 24 hours at 37^0C in CO_2 incubator. After the incubation, the cells that had migrated to the outer surface of the inserts were fixed using 4% paraformaldehyde for 10 minutes and stained using 5% crystal violet stain in Methanol for 1 hour. The number of cells migrated were imaged using Zeiss Axiovert microscope under a 10X objective and number of cells in an image were quantified using multipoint selection tool of ImageJ and averaged. Average number of cells migrated in two different experiments were plotted using GraphPad Prism software.

Chromatin immunoprecepitation (ChIP) Experiments

ChIP experiments were done as described (Zargar *et al*., 2018) with some minor modifications. Following antibodies were used for our ChIP assays, H3K4Me2 (Abcam 32356), H3K4Me3 (Millipore 07-473 or Abcam 8580), H3 (Abcam 1791), IgG (Millipore 12-370). qRT PCR was done to calculate Ct values. Percentage enrichment over the Input was calculated using the formulae percentage enrichment = 100* 2^{x-y} where x is the Ct value for Input adjusted for dilution factor and y is the Ct value for the IP samples. For ChIP in MLL iKO cells, Fold over control was calculated using the formulae 2^{x-y} of test/2^{x-y} of control, where x and y are Ct values of input and IP. ABI 7500 system was used for qRT-PCR. Primer sequences used are listed in the supplementary data Table 2.

Animal experiments

All the animal experiments were performed after being approved by CDFD institutional animal ethics committee (Protocol number EAF/ST/25/2021). 6-8 weeks old $FOXN1^{-/-}$ female nude mice were used for the studies. For xenograft assays, MDA-MB-231 cells were transduced with control, MLL or RhoGDI1 shRNA containing lentiviruses and subjected to

brief Puromycin (4µg/ml) treatment after 24 hours. 48 hours post transduction, 10^6 cells suspended in 100µl of 1:1 mixture of Matrigel (Corning 354254) and PBS were injected subcutaneously in one of the breasts of each female nude mice. Tumor growth was monitored every 10 days. Mice were sacrificed and tumors were harvested on the 40^{th} day and their weights were measured. For OICR-9429 treatment, study was done as described previously (Zhou *et al.*, 2021). Tumors were induced in female nude mice as explained above using MDA-MB-231 cells. When tumors reached the size of 50 mm^3 (approximately 1 week), mice were grouped randomly. One group of mice was administered 4 mg/Kg OICR-9429 and the other with DMSO intravenously for 7 alternate days. Mice were sacrificed after 40 days from the beginning of experiment. Tumors were harvested and their weights were measured. The injections were performed by CDFD animal facility staff, who were blinded for the study.

Statistical Analysis

For all the statistical analyses, 95% confidence interval was applied. GraphPad Prism software was used to determine statistical significance. For simple comparison between two sets, Student's unpaired t test was applied. For multiple comparisons, one way or two way ANOVA test was implemented as indicated. Significance of each test is mentioned in the respective figure legends in the form of P values.

Acknowledgements

We thank A. Karole for cloning control and MLL shRNAs; I. Kaur for sharing time on Li-cor Imaging system. A.N.C. is recipients of Junior and Senior Research Fellowships of the University Grants Commission, India toward the pursuit of a PhD degree of the Manipal University. K.A.L. is recipients of Junior and Senior Research Fellowships of Council of Scientific and Industrial Research, India toward the pursuit of a PhD degree of Regional

Centre for Biotechnology. This work was supported in part by a grant from Department of Biotechnology (DBT) to S.T. (BT/PR334385/BRB/10/1829/2019), Department of Science and Technology to S.T. (EMR/2016/000406), DBT/Wellcome Trust India Alliance Senior Fellowship to S.T.[IA/S/18/2/503981] and CDFD core funds.

Author contributions

A. N.C. performed all experiments except the ones mentioned below. K.A.L. performed experiments presented in Figures 6 and S6. K.A.L also generated the MLL iKO in HEK-293 cell line. S.T. and A.N.C. designed and analyzed the experiments and wrote the manuscript.

Conflict of Interest

The authors declare that they have no conflict of interest.

References

Ali, A., Veeranki, S. N. and Tyagi, S. (2014). A SET-domain-independent role of WRAD complex in cell-cycle regulatory function of mixed lineage leukemia. *Nucleic Acids Res.* **42**, 7611–7624.

Ali, A., Veeranki, S. N., Chinchole, A. and Tyagi, S. (2017). MLL/WDR5 Complex Regulates Kif2A Localization to Ensure Chromosome Congression and Proper Spindle Assembly during Mitosis. *Dev. Cell* **41**, 605-622.e7.

Ansari, K. I., Kasiri, S. and Mandal, S. S. (2013). Histone methylase MLL1 has critical roles in tumor growth and angiogenesis and its knockdown suppresses tumor growth in vivo. *Oncogene* **32**, 3359–3370.

Azim, A. C., Barkalow, K., Chou, J. and Hartwig, J. H. (2000). Activation of the small GTPases, rac and cdc42, after ligation of the platelet PAR-1 receptor. *Blood* **95**, 959–64.

Barski, A., Cuddapah, S., Cui, K., Roh, T.-Y., Schones, D. E., Wang, Z., Wei, G., Chepelev, I. and Zhao, K. (2007). High-resolution profiling of histone methylations in the human genome. *Cell* **129**, 823–37.

Betapudi, V., Licate, L. S. and Egelhoff, T. T. (2006). Distinct roles of nonmuscle myosin II isoforms in the regulation of MDA-MB-231 breast cancer cell spreading and migration. *Cancer Res.* **66**, 4725–33.

Blanchoin, L., Boujemaa-Paterski, R., Sykes, C. and Plastino, J. (2014). Actin dynamics, architecture, and mechanics in cell motility. *Physiol. Rev.* **94**, 235–263.

Boulter, E., Garcia-Mata, R., Guilluy, C., Dubash, A., Rossi, G., Brennwald, P. J. and Burridge, K. (2010). Regulation of Rho GTPase crosstalk, degradation and activity by RhoGDI1. *Nat. Cell Biol.* **12**, 477–483.

Carugo, A., Genovese, G., Seth, S., Nezi, L., Rose, J. L., Bossi, D., Cicalese, A., Shah, P. K., Viale, A., Pettazzoni, P. F., et al. (2016). In Vivo Functional Platform Targeting Patient-Derived Xenografts Identifies WDR5-Myc Association as a Critical Determinant of Pancreatic Cancer. *Cell Rep.* **16**, 133–147.

Cho, H. J., Kim, J. T., Lee, S. J., Hwang, Y. S., Park, S. Y., Kim, B. Y., Yoo, J., Hong, K. S., Min, J. K., Lee, C. H., et al. (2018). Protein phosphatase 1B dephosphorylates Rho guanine nucleotide dissociation inhibitor 1 and suppresses cancer cell migration and invasion. *Cancer Lett.* **417**, 141–151.

Cohn, M. J., Patel, K., Krumlauf, R., Wilkinson, D. G., Clarke, J. D. and Tickle, C. (1997). Hox9 genes and vertebrate limb specification. *Nature* **387**, 97–101.

Dangi, C. B. S. and Firodiya, A. (2012). Triple-negative breast cancer and it's therapeutic options. *Int. J. Pharma Bio Sci.* **3**, 130–160.

Ernst, P., Wang, J., Huang, M., Goodman, R. H. and Korsmeyer, S. J. (2001). MLL and CREB bind cooperatively to the nuclear coactivator CREB-binding protein. *Mol. Cell. Biol.* **21**, 2249–2258.

Etienne-Manneville, S. and Hall, A. (2002). Rho GTPases in cell biology. *Nature* **420**, 629–635.

Fritz, G., Just, I. and Kaina, B. (1999). Proteomics of breast cancer for marker discovery and signal pathway profiling. *Int. J. Cancer* **81**, 682–687.

Goitre, L., Trapani, E., Trabalzini, L. and Retta, S. F. (2014). The ras superfamily of small GTPases: The unlocked secrets. *Methods Mol. Biol.* **1120**, 1–18.

Golding, A. E., Visco, I., Bieling, P. and Bement, W. M. (2019). Extraction of active rhoGTPases by rhoGDI regulates spatiotemporal patterning of rhogtpases. *Elife* **8**, 1–26.

Gorvel, J. P., Chang, T. C., Boretto, J., Azuma, T. and Chavrier, P. (1998). Differential properties of D4/LyGDI versus RhoGDI: phosphorylation and rho GTPase selectivity. *FEBS Lett.* **422**, 269–73.

Grebien, F., Vedadi, M., Getlik, M., Giambruno, R., Grover, A., Avellino, R., Skucha, A., Vittori, S., Kuznetsova, E., Smil, D., et al. (2015a). Pharmacological targeting of the Wdr5-MLL interaction in C/EBPα N-terminal leukemia. *Nat. Chem. Biol.* **11**, 571–578.

Grebien, F., Vedadi, M., Getlik, M., Giambruno, R., Grover, A., Avellino, R., Skucha, A., Vittori, S., Kuznetsova, E., Smil, D., et al. (2015b). Erratum: Pharmacological targeting of the Wdr5-MLL interaction in C/EBPα N-terminal leukemia. *Nat. Chem. Biol.* **11**, 815.

Guo, F., Debidda, M., Yang, L., Williams, D. A. and Zheng, Y. (2006). Genetic deletion of Rac1 GTPase reveals its critical role in actin stress fiber formation and focal adhesion complex assembly. *J. Biol. Chem.* **281**, 18652–18659.

He, F. X., Zhang, L. L., Jin, P. F., Liu, D. D. and Li, A. H. (2019). DPY30 regulates cervical squamous cell carcinoma by mediating epithelial-mesenchymal transition (EMT). *Onco. Targets. Ther.* **12**, 7139–7147.

Hess, J. L., Yu, B. D., Li, B., Hanson, R. and Korsmeyer, S. J. (1997). Defects in yolk sac hematopoiesis in Mll-null embryos. *Blood* **90**, 1799–806.

Hodge, R. G. and Ridley, A. J. (2016). Regulating Rho GTPases and their regulators. *Nat. Rev. Mol. Cell Biol.* **17**, 496–510.

Hondermarck, H., Vercoutter-Edouart, A. S., Révillion, F., Lemoine, J., El-Yazidi-Belkoura, I., Nurcombe, V. and Peyrat, J. P. (2001). Proteomics of breast cancer for marker discovery and signal pathway profiling. *Proteomics* **1**, 1216–1232.

Hsieh, J. J.-D., Ernst, P., Erdjument-Bromage, H., Tempst, P. and Korsmeyer, S. J. (2003). Proteolytic cleavage of MLL generates a complex of N- and C-terminal fragments that confers protein stability and subnuclear localization. *Mol. Cell. Biol.* **23**, 186–194.

Ito, H., Morishita, R. and Nagata, K.-I. (2018). Functions of Rhotekin, an Effector of Rho GTPase, and Its Binding Partners in Mammals. *Int. J. Mol. Sci.* **19**,.

Jaffe, A. B. and Hall, A. (2005). Rho GTPases: Biochemistry and biology. *Annu. Rev. Cell Dev. Biol.* **21**, 247–269.

Jakobs, M. A., Dimitracopoulos, A. and Franze, K. (2019). KymoButler, a deep learning software for automated kymograph analysis. *Elife* **8**,.

Jung, H., Yoon, S. R., Lim, J., Cho, H. J. and Lee, H. G. (2020). Dysregulation of rho gtpases in human cancers. *Cancers (Basel).* **12**, 1–17.

Kovac, B., Teo, J. L., Mäkelä, T. P. and Vallenius, T. (2013). Assembly of non-contractile dorsal stress fibers requires α-actinin-1 and Rac1 in migrating and spreading cells. *J. Cell Sci.* **126**, 263–73.

Livak, K. J. and Schmittgen, T. D. (2001). Analysis of relative gene expression data using real-time quantitative PCR and the 2(-Delta Delta C(T)) Method. *Methods* **25**, 402–8.

Luxenburg, C. and Zaidel-Bar, R. (2019). From cell shape to cell fate via the cytoskeleton — Insights from the epidermis. *Exp. Cell Res.* **378**, 232–237.

Malek, R., Gajula, R. P., Williams, R. D., Nghiem, B., Simons, B. W., Nugent, K., Wang, H., Taparra, K., Lemtiri-Chlieh, G., Yoon, A. R., et al. (2017). TWIST1-WDR5-hottip regulates Hoxa9 chromatin to facilitate prostate cancer metastasis. *Cancer Res.* **77**, 3181–3193.

Marschalek, R. (2016). Classification of mixed-lineage leukemia fusion partners predicts additional cancer pathways. *Ann. Lab. Med.* **36**, 85–100.

Miura, Y., Kikuchi, A., Musha, T., Kuroda, S., Yaku, H., Sasaki, T. and Takai, Y. (1993). Regulation of morphology by rho p21 and its inhibitory GDP/GTP exchange protein (rho GDI) in Swiss 3T3 cells. *J. Biol. Chem.* **268**, 510–515.

Navarro-Lérida, I., Sánchez-Álvarez, M. and del Pozo, M. Á. (2021). Post-Translational Modification and Subcellular Compartmentalization: Emerging Concepts on the Regulation and Physiopathological Relevance of RhoGTPases. *Cells* **10**, 1990.

Nobes, C. D. and Hall, A. (1995). Rho, Rac, and Cdc42 GTPases regulate the assembly of multimolecular focal complexes associated with actin stress fibers, lamellipodia, and filopodia. *Cell* **81**, 53–62.

Ota, T., Maeda, M., Murakami, M., Takegami, T., Suto, S. and Tatsuka, M. (2007). Activation of Rac1 by Rho-guanine nucleotide dissociation inhibitor-beta with defective isoprenyl-binding pocket. *Cell Biol. Int.* **31**, 92–6.

Paluch, E. and Heisenberg, C. P. (2009). Biology and Physics of Cell Shape Changes in Development. *Curr. Biol.* **19**, R790–R799.

Pascual-Vargas, P., Cooper, S., Sero, J., Bousgouni, V., Arias-Garcia, M. and Bakal, C. (2017). RNAi screens for Rho GTPase regulators of cell shape and YAP/TAZ localisation in triple negative breast cancer. *Sci. Data* **4**, 1–13.

Patel, A., Dharmarajan, V., Vought, V. E. and Cosgrove, M. S. (2009). On the mechanism of multiple lysine methylation by the human mixed lineage leukemia protein-1 (MLL1) core complex. *J. Biol. Chem.* **284**, 24242–24256.

Pillé, J. Y., Denoyelle, C., Varet, J., Bertrand, J. R., Soria, J., Opolon, P., Lu, H., Pritchard, L. L., Vannier, J. P., Malvy, C., et al. (2005). Anti-RhoA and Anti-RhoC siRNAs inhibit the proliferation and invasiveness of MDA-MB-231 breast cancer cells in vitro and in vivo. *Mol. Ther.* **11**, 267–274.

Pollard, T. D. and Cooper, J. A. (2009). Actin, a central player in cell shape and movement. *Science (80-.).* **326**, 1208–1212.

Radjabi, A. R., Sawada, K., Jagadeeswaran, S., Eichbichler, A., Kenny, H. A., Montag, A., Bruno, K. and Lengyel, E. (2008). Thrombin induces tumor invasion through the induction and association of matrix metalloproteinase-9 and β1-integrin on the cell surface. *J. Biol. Chem.* **283**, 2822–2834.

Raftopoulou, M. and Hall, A. (2004). Cell migration: Rho GTPases lead the way. *Dev. Biol.* **265**, 23–32.

Reymond, N., Riou, P. and Ridley, A. J. (2012a). Rho GTPases and cancer cell transendothelial migration. *Methods Mol. Biol.* **827**, 123–142.

Reymond, N., Im, J. H., Garg, R., Vega, F. M., Borda d'Agua, B., Riou, P., Cox, S., Valderrama, F., Muschel, R. J. and Ridley, A. J. (2012b). Cdc42 promotes transendothelial migration of cancer cells through β1 integrin. *J. Cell Biol.* **199**, 653–68.

Ridley, A. J. and Hall, A. (1992). The small GTP-binding protein rho regulates the assembly of focal adhesions and actin stress fibers in response to growth factors. *Cell* **70**, 389–399.

Ridley, A. J., Paterson, H. F., Johnston, C. L., Diekmann, D. and Hall, A. (1992). The small GTP-binding protein rac regulates growth factor-induced membrane ruffling. *Cell* **70**, 401–410.

Ridley, A. J., Schwartz, M. A., Burridge, K., Firtel, R. A., Ginsberg, M. H., Borisy, G., Parsons, J. T. and Horwitz, A. R. (2003). Cell migration: integrating signals from front to back. *Science* **302**, 1704–9.

Riedl, J., Crevenna, A. H., Kessenbrock, K., Yu, J. H., Neukirchen, D., Bista, M., Bradke, F., Jenne, D., Holak, T. A., Werb, Z., et al. (2008). Lifeact: a versatile marker to visualize F-actin. *Nat. Methods* **5**, 605–7.

Sailem, H., Bousgouni, V., Cooper, S. and Bakal, C. (2014). Cross-talk between Rho and Rac GTPases drives deterministic exploration of cellular shape space and morphological heterogeneity.

Sanjana, N. E., Shalem, O. and Zhang, F. (2014). Improved vectors and genome-wide libraries for CRISPR screening. *Nat. Methods* **11**, 783–784.

Shi, G. X., Yang, W. S., Jin, L., Matter, M. L. and Ramos, J. W. (2017). RSK2 drives cell motility by serine phosphorylation of LARG and activation of Rho GTPases. *Proc. Natl. Acad. Sci. U. S. A.* **115**, E190–E199.

Steffen, A., Rottner, K., Ehinger, J., Innocenti, M., Scita, G., Wehland, J. and Stradal, T. E. B. (2004). Sra-1 and Nap1 link Rac to actin assembly driving lamellipodia formation. *EMBO J.* **23**, 749–59.

Stringer, B. W., Day, B. W., D'Souza, R. C. J., Jamieson, P. R., Ensbey, K. S., Bruce, Z. C., Lim, Y. C., Goasdoué, K., Offenhäuser, C., Akgül, S., et al. (2019). A reference collection of patient-derived cell line and xenograft models of proneural, classical and mesenchymal glioblastoma. *Sci. Rep.* **9**, 4902.

Thiel, A. T., Blessington, P., Zou, T., Feather, D., Wu, X., Yan, J., Zhang, H., Liu, Z., Ernst, P., Koretzky, G. A., et al. (2010). MLL-AF9-induced leukemogenesis requires coexpression of the wild-type Mll allele. *Cancer Cell* **17**, 148–59.

Tregnago, C., Ros, A. Da, Porcù, E., Benetton, M., Simonato, M., Simula, L., Borella, G., Polato, K., Minuzzo, S., Borile, G., et al. (2020). Thioridazine requires calcium influx to induce MLL-AF6-rearranged AML cell death. *Blood Adv.* **4**, 4417–4429.

Tyagi, S. and Herr, W. (2009). E2F1 mediates DNA damage and apoptosis through HCF-1 and the MLL family of histone methyltransferases. *EMBO J.* **28**, 3185–95.

Van Lidth de Jeude, J. F., Vermeulen, J. L. M., Montenegro-Miranda, P. S., Van den Brink, G. R. and Heijmans, J. (2015). A protocol for lentiviral transduction and downstream analysis of intestinal organoids. *J. Vis. Exp.*

van Nieuw Amerongen, G. P., van Delft, S., Vermeer, M. A., Collard, J. G. and van Hinsbergh, V. W. (2000). Activation of RhoA by thrombin in endothelial hyperpermeability: role of Rho kinase and protein tyrosine kinases. *Circ. Res.* **87**, 335–40.

Vega, F. M., Fruhwirth, G., Ng, T. and Ridley, A. J. (2011). RhoA and RhoC have distinct roles in migration and invasion by acting through different targets. *J. Cell Biol.* **193**, 655–665.

Wang, P., Lin, C., Smith, E. R., Guo, H., Sanderson, B. W., Wu, M., Gogol, M., Alexander, T., Seidel, C., Wiedemann, L. M., et al. (2009). Global Analysis of H3K4 Methylation Defines MLL Family Member Targets and Points to a Role for MLL1-Mediated H3K4 Methylation in the Regulation of Transcriptional Initiation by RNA Polymerase II. *Mol. Cell. Biol.* **29**, 6074–6085.

Wang, T., Wei, J. J., Sabatini, D. M. and Lander, E. S. (2014). Genetic screens in human cells using the CRISPR-Cas9 system. *Science* **343**, 80–4.

Worthylake, R. A., Lemoine, S., Watson, J. M. and Burridge, K. (2001). RhoA is required for monocyte tail retraction during transendothelial migration. *J. Cell Biol.* **154**, 147–160.

Yang, W., Trahan, G. D., Howell, E. D., Speck, N. A., Jones, K. L., Gillen, A. E., Riemondy, K., Hesselberth, J., Bryder, D. and Ernst, P. (2020). Enhancing Hematopoiesis from Murine Embryonic Stem Cells through MLL1-Induced Activation of a Rac/Rho/Integrin Signaling Axis. *Stem Cell Reports* **14**, 285–299.

Ye, X., Zhang, R., Lian, F., Zhang, W., Lu, W., Han, J., Zhang, N., Jin, J., Luo, C., Chen, K., et al. (2019). The identification of novel small-molecule inhibitors targeting WDR5-MLL1 interaction through fluorescence polarization based high-throughput screening. *Bioorganic Med. Chem. Lett.* **29**, 638–645.

Yu, B. D., Hanson, R. D., Hess, J. L., Horning, S. E. and Korsmeyer, S. J. (1998). MLL, a mammalian trithorax-group gene, functions as a transcriptional maintenance factor in morphogenesis. *Proc. Natl. Acad. Sci. U. S. A.* **95**, 10632–6.

Yu, J., Zhang, D., Liu, J., Li, J., Yu, Y., Wu, X. R. and Huang, C. (2012). RhoGDI SUMOylation at Lys-138 increases its binding activity to Rho GTPase and its inhibiting cancer cell motility. *J. Biol. Chem.* **287**, 13752–13760.

Zargar, Z. U., Kimidi, M. R. and Tyagi, S. (2018). Dynamic site-specific recruitment of RBP2 by pocket protein p130 modulates H3K4 methylation on E2F-responsive promoters. *Nucleic Acids Res.* **46**, 174–188.

Zhang, P. and Bergamin, E. (2012). Review Review The Many Facets of MLL1 Regulation The Many Facets of MLL1 Regulation. **99**, 136–145.

Zhang, B., Zhang, Y., Dagher, M. C. and Shacter, E. (2005). Rho GDP dissociation inhibitor protects cancer cells against drug-induced apoptosis. *Cancer Res.* **65**, 6054–6062.

Zhang, Y., Ji, T., Ma, S. and Wu, W. (2020). MLL1 promotes migration and invasion of fibroblast-like synoviocytes in rheumatoid arthritis by activating the TRIF/NF-κB signaling pathway via H3K4me3 enrichment in the TLR4 promoter region. *Int. Immunopharmacol.* **82**, 106220.

Zhou, Y. T., Chew, L. L., Lin, S. and Low, B. C. (2010). The BNIP-2 and Cdc42GAP homology (BCH) domain of p50RhoGAP/Cdc42GAP sequesters RhoA from inactivation by the adjacent GTPase-activating protein domain. *Mol. Biol. Cell* **21**, 3232–46.

Zhou, Q., Chen, X., He, H., Peng, S., Zhang, Y., Zhang, J., Cheng, L., Liu, S., Huang, M., Xie, R., et al. (2021). WD repeat domain 5 promotes chemoresistance and Programmed Death-Ligand 1 expression in prostate cancer. *Theranostics* **11**, 4809–4824.

Zmurchok, C. and Holmes, W. R. (2020). Simple Rho GTPase Dynamics Generate a Complex Regulatory Landscape Associated with Cell Shape. *Biophys. J.* **118**, 1438–1454.

Figures

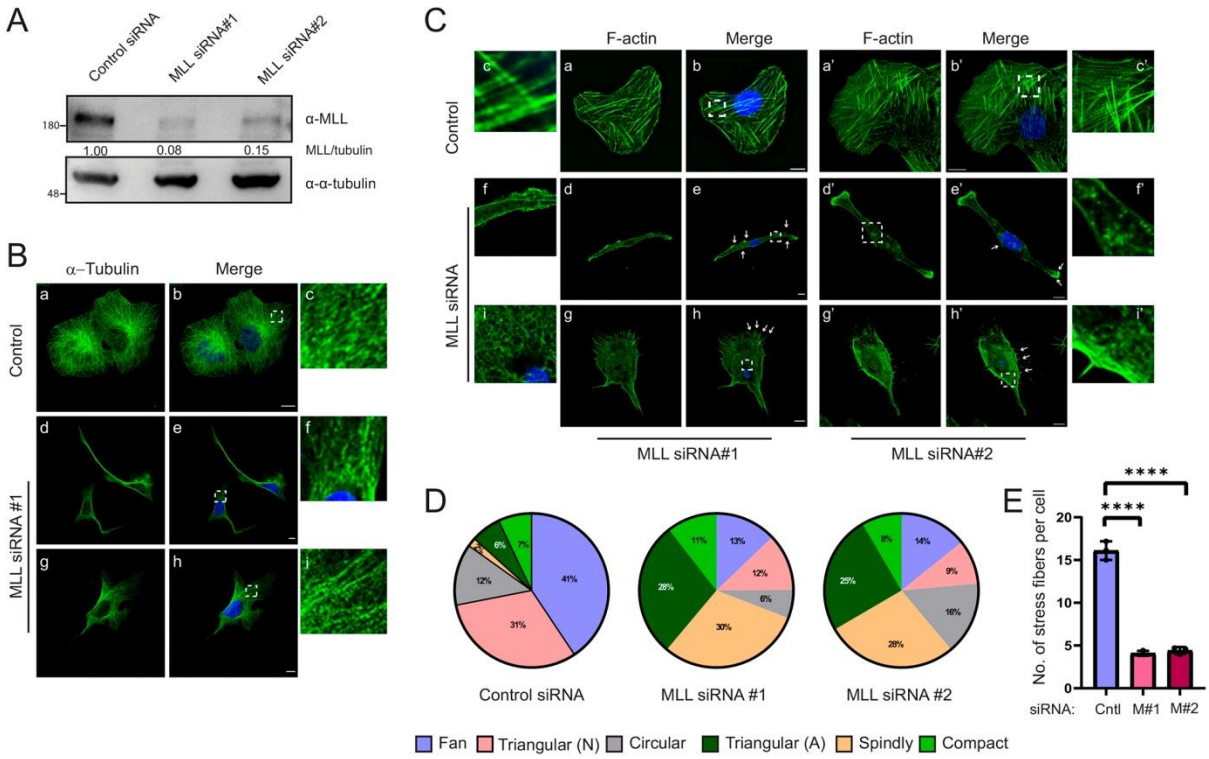

Fig. 1. Loss of MLL affects cell shape and actin cytoskeleton.

(A) U-2OS cells, treated with control, MLL siRNA#1 and MLL siRNA#2 for 72 hr., were lysed and immunoblotted. Blots were probed with anti-MLL and anti-α tubulin antibody as indicated. **(B,C)** Control and MLL siRNA-treated U-2OS cells were fixed and used for immunofluorescence (IF). Cells were stained using anti-α tubulin (**B,** green) antibody or rhodamine-conjugated phalloidin (**C,** green). Nucleus was stained using 4', 6'-dia-midino 2-phenylindole (DAPI, blue). White arrows in **C,** panel e indicate small protrusions and panel h indicate spine like actin rich filopodia. Panel c, f, i, c', f' and i' show insets of the region highlighted in panel b, e, h, b', e' and h' respectively. Scale bar, 10 μm. **(D,E)** Shape of the cells (**D**) or number of stress fibers (**E**) treated with different siRNAs from **(C)** were quantified from 3 independent experiments as shown. (**E**) Data represents mean ± SD. ****P < .0001, one-way ANOVA test. F-actin, filamentous-actin; Cntl, control; M#1, MLL siRNA#1; M#2, MLL siRNA#2.

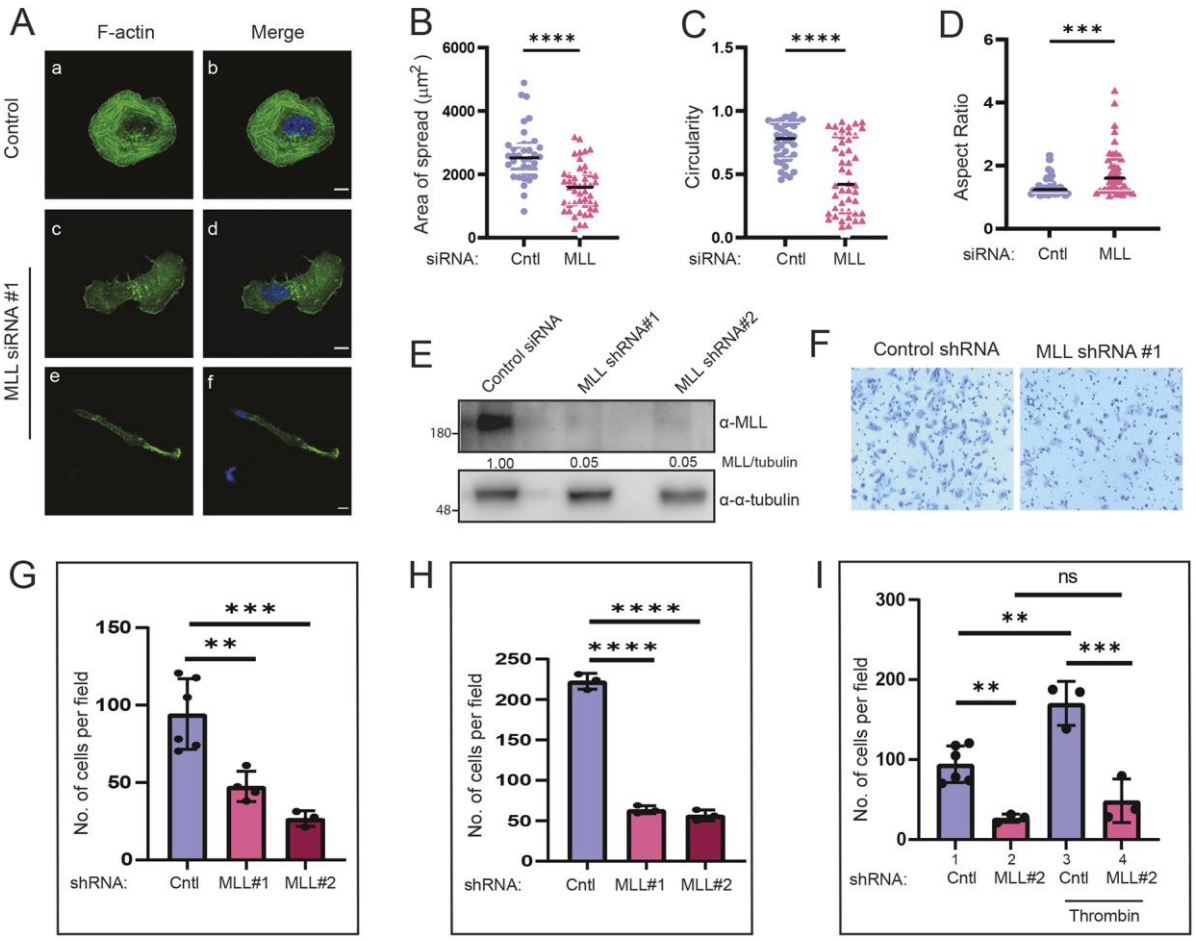

Fig. 2. Depletion of MLL alters cell-spreading and cell migration.

(A) Representative IF image of U-2OS cells, treated with control or MLL siRNA#1 for 72 hr., and plated on fibronectin coated cover slips for 4 hr., are shown. Phalloidin (green) and DAPI (blue) staining is shown. Scale bar, 10 μm. (**B**-**D**) Quantifications of area of spread (**B**), circularity (**C**) and aspect ratio (**D**) of control or MLL siRNA-treated cells are shown. Data are represented as violin plot with all the data points and a median. **** P <.0001, ***P<.0004 (Student's unpaired t-test; n = 40 cells and m =2 experiments). **(E)** Shown are immunoblots, probed with anti-MLL and anti-tubulin antibody, of U-2OS cells treated with two different MLL shRNAs. (**F**) U-2OS cells were treated with control or MLL shRNA#1 for 48 hr. and transwell migration (Boyden chamber) assay was performed. Bright field images show migrated cells upon treatment with respective shRNAs as indicated. (**G**, **H**) Quantifications for number of U-2OS (**G**) and MDA-MB -231(**H**) cells migrated per field are shown. Data are represented as mean ± SD. **P =.0046 and ***P =.0006 (**G**) and ****P <0.0001 (**H**) respectively. (one-way ANOVA; m=3 experiments). **(I)** U-2OS cells treated with control or MLL shRNA#2 were incubated in media containing thrombin (4U / ml) for

48 hr. and seeded for transwell migration assay. Quantifications for number of cells migrated per field is shown. For ease of comparison, data from **(G)** of control and MLL shRNA#2 treatments is replotted here. Data are represented as mean ± SD. **P = .007 (lane 1) and .003 (lane 3) respectively, ***P = .0002 and ns P = .65, (one-way ANOVA test; m=3 experiments).

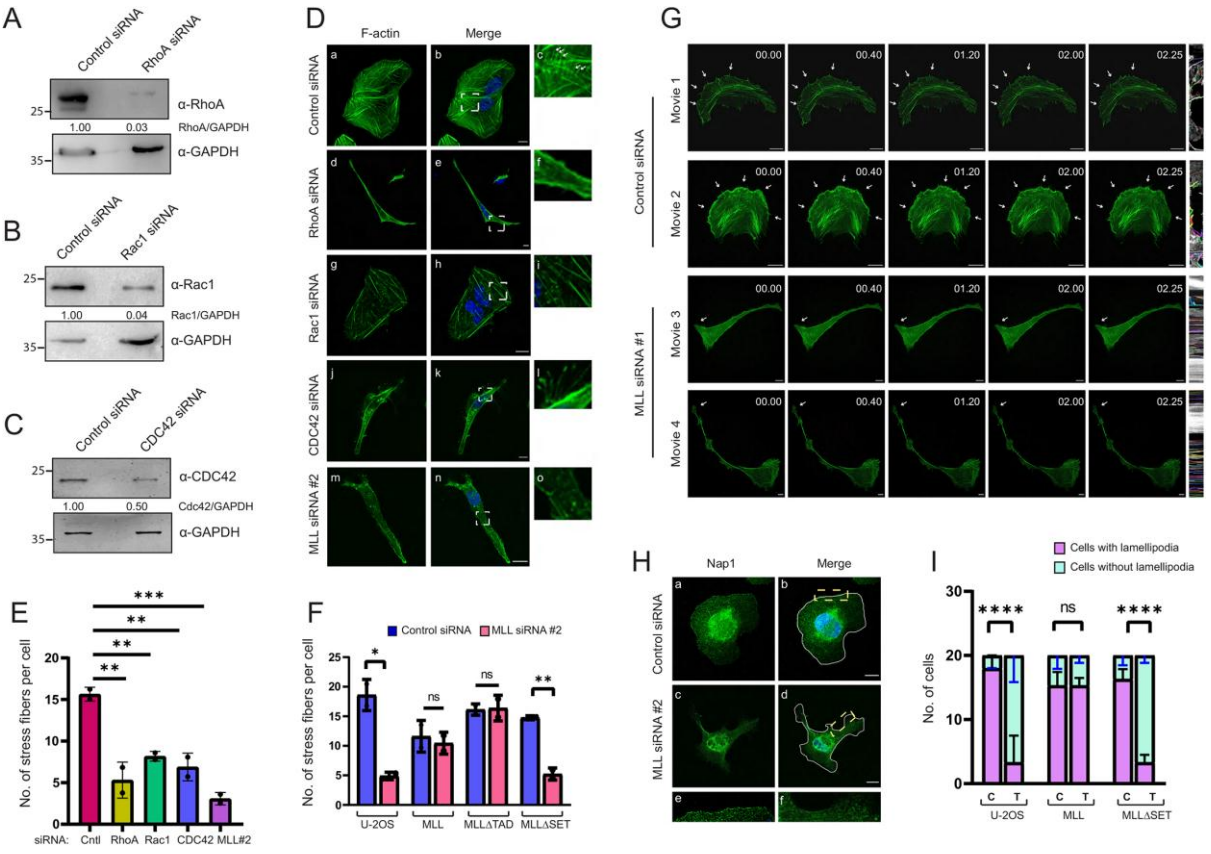

Fig. 3. MLL/Rho GTPases depletion causes loss of actin dynamics and lamellipodia formation.

(**A-C**) Immunoblot of whole cell lysates of U-2OS cells treated with control, RhoA, Rac1 and CDC42 siRNA and probed with respective antibodies are shown. GAPDH was used as loading control as shown. (**D**) IF of U-2OS cells treated with indicated siRNAs for 72 hr. is shown. The cells were stained with phalloidin(green) and DAPI (blue). White arrows in panel c indicate fine actin stress fibers. (**E**) Quantification of number of stress fibers in cells treated with respective siRNAs from **D.** Data are represented as mean ± SD. ***P <.001, **P =.001 (RhoA), .003(Rac1) and .001(CDC42) (one-way ANOVA; n = 40 cells and m = 2 experiments). (**F**) Quantification of number of stress fibers in U-2OS cells, and U-2OS expressing various mutants of MLL, treated with control or MLL#2 siRNA is shown. Data in wild type U-2OS is same as **E**, and replotted here. Data represents mean ± SD. **P =.006, *P =.019, ns=.66 (MLL) and .89 (MLLΔTAD) (Student's unpaired t test; n = 40 cells and m = 2 experiments). (**G**) U-2OS cells expressing GFP-Lifeact were treated with control or MLL#1 siRNA for 72 hr., then imaged in SIM time-lapse mode at 5 seconds interval. Representative images are shown with time indicated in mm:ss format (Also see Movie 1-4). White arrows in the panels highlight region with high actin dynamics. Kymographs are shown on left and

the coloured lines therein indicate the particles selected for quantifying the average track velocities. **(H)** Formation of lamellipodia in control (panels a and b) and MLL-depleted (panels c and d) U-2OS cells. Cell boundaries are marked in white in panel b and d while insets of the region highlighted are shown in panel e and f. (**I**) Number of cells with and without lamellipodia were quantified in cells treated with control or MLL#2 siRNA. Data represents mean ± SD. ****P < .0001, ns P >.99. Downward error bars are shown for cells without lamellipodia and upward error bars for cells with lamellipodia. (Two-way ANOVA test; n = 60 cells and m = 3 experiments). (**D, G -H**) Scale bar, 10 μm. C denotes control and T denotes MLL siRNA treatment; ΔTAD, Trans activation domain deletion; ΔSET, SET domain deletion.

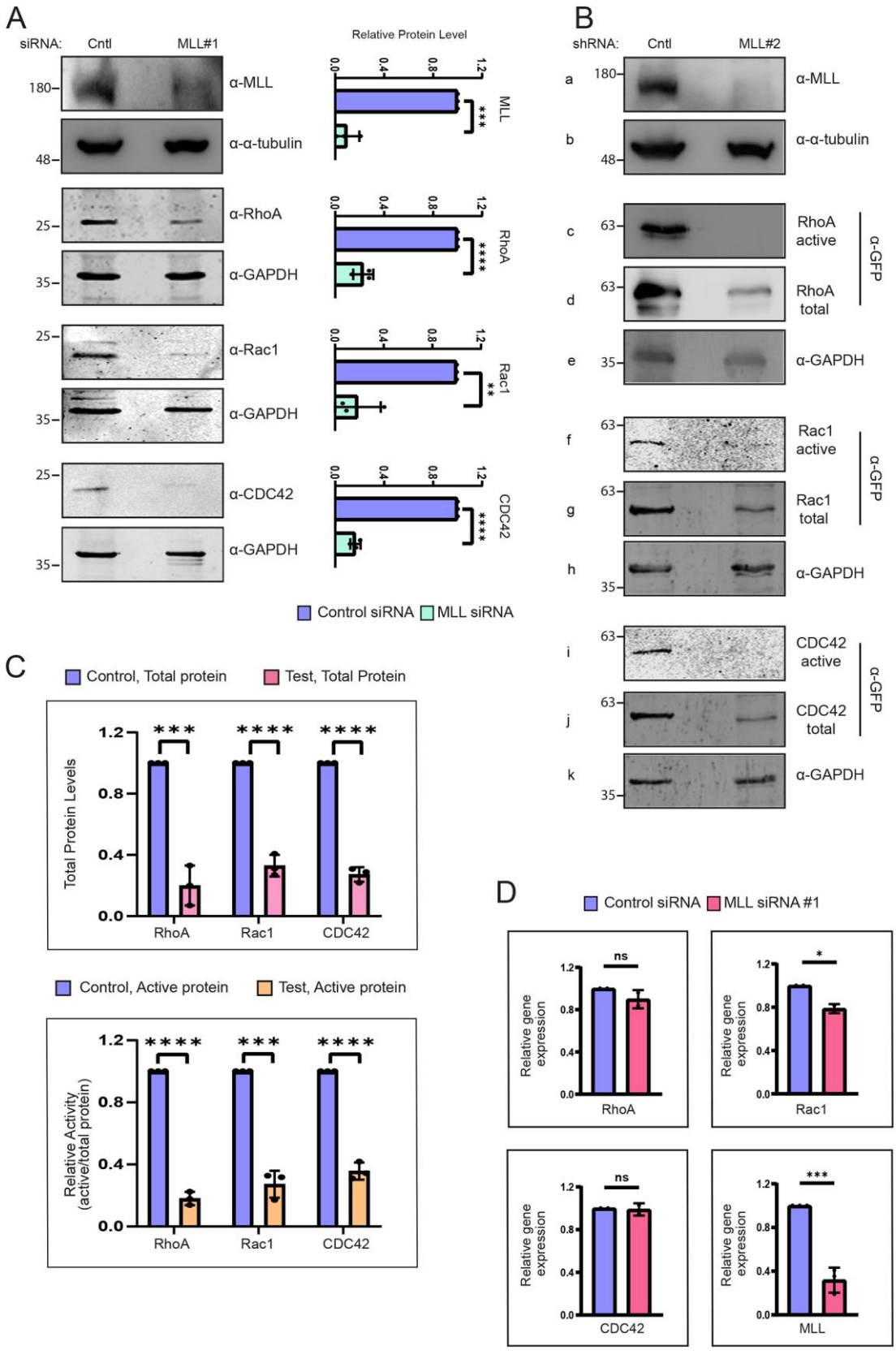

Fig. 4. Loss of MLL affects stability and activity of Rho GTPases.

(**A**) Immunoblots of U-2OS cells, treated with control or MLL#1 siRNA, probed with indicated antibodies, are shown. Graphs on the right show the relative protein levels (with respect to loading control). Data represents mean ± SD. ****P< .0001 for RhoA and CDC42 respectively, ***P= .0001 and **P= .0017 for MLL and Rac1 respectively. (Student's unpaired t-test, m = 3 experiments). (**B**) U-2OS cells stably expressing GFP tagged RhoA, Rac1 or CDC42 were either treated with control or MLL shRNA#2 for 72 hr. The cells were then lysed and subjected to pull-down using GST tagged effector domains (see Methods). Immunoblot analysis indicate endogenous protein levels of MLL (panel a) and α-tubulin (panel b). Total protein levels (panels d, g and j) and active (GTP-bound) protein levels (panels c, f and i) of indicated Rho GTPases, probed with anti GFP antibody are shown. Panels e, h and k, were probed with anti-GAPDH antibody. (**C**) Densitometric analyses of immunoblots from (**B**) of total protein levels relative to loading control (upper panel) and relative activity (ratio of active to total protein levels) upon depletion of MLL are shown. Data represents mean ± SD. ****P<.0001, ***P<.005 (Student's unpaired t-test, m = 3 experiments). (**D**) Real time quantitative PCR (RT-qPCR) analysis of gene expression upon MLL depletion is shown. Relative gene expression was calculated using -ΔΔct method. Data represents mean ± SD. *P =.018 (Rac1) and ***P<.001 (MLL), ns P=.23 (RhoA) and .80 (CDC42). (Student's unpaired t-test m = 2 experiments.) (**A**-**B**), numbers on the left indicate molecular weight markers in kDa.

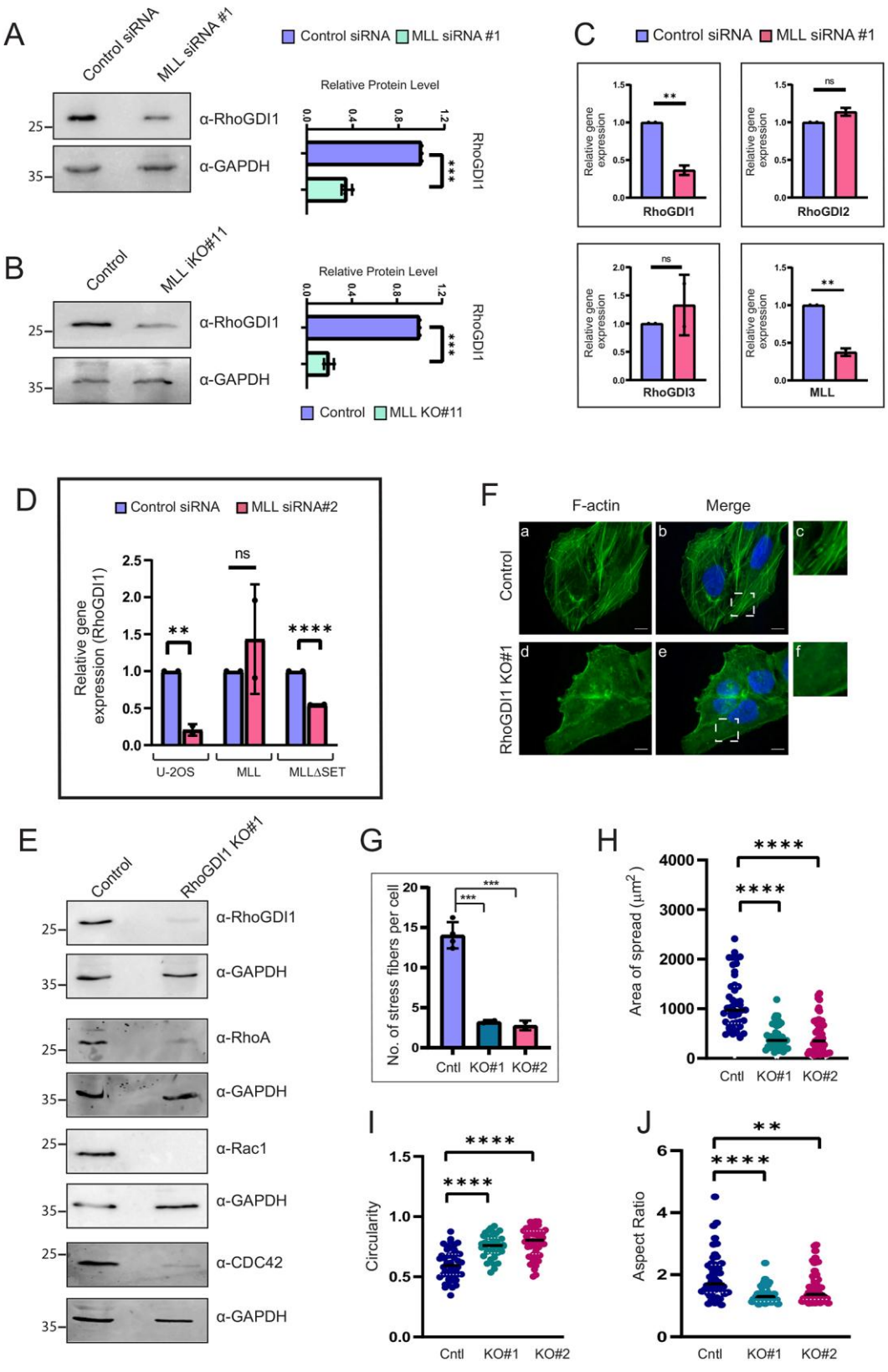

Fig. 5. Down regulation of MLL affects the protein and transcript levels of RhoGDI1.

(**A-B**) Whole cell lysates from control and MLL-depleted U-2OS cells (**A**) and HEK-293 control (Cas9-expressing cells were used as control) and MLL iKO(#11) clonal cell line (**B**) were immunoblotted and probed with RhoGDI1 and GAPDH. Graphs indicate the quantifications of relative protein levels shown in **A** and **B**. Data represents mean ± SD. ****P< .0001 **A**, ***P= .0009 **B**. (Student's unpaired t-test m=3 experiments) **(C)** RT-qPCR analysis of gene expression upon MLL siRNA-depletion is shown. Data represents mean ± SD, **P=.005 (RhoGDI1), .003 (MLL); P =.06 (RhoGDI2) and .47 (RhoGDI3) (Student's unpaired t-test; m=2 experiments). **(D)** RT-qPCR analysis of gene expression of RhoGDI1 in wild type U-2OS and U-2OS cells stably expressing various mutants of MLL upon depletion of endogenous MLL using siRNA#2 is shown. Data represents mean ± SD. P =.50 for MLL, ** P=.005 and **** P <.0001 (Student's unpaired t-test; m = 2 experiments). **(E)** Whole cell lysates of control U-2OS and RhoGDI1 knock out (KO#1) cells were immunoblotted and probed as shown. **(F)** IF image of control U-2OS and RhoGDI1 KO#1 cells are shown. Cells are stained with phalloidin. Scale bar, 10 μm. **(G)** Quantification for number of stress fibers per cell in control U-2OS, RhoGDI1 KO #1 and #2 clonal cell lines is shown. Data represents mean ± SD, ***P<.001 (one-way ANOVA test; n=80 cells and m=4 experiments for control and n= 40 cells and m = 2 experiments for RhoGDI1 KO clone #1 and #2). **(H-J)** Quantification of area of spread **(H)**, circularity **(I)** and aspect ratio **(J)** of U-2OS and RhoGDI1 KO clones #1 and #2 spread on fibronectin coated cover slips. **** P <.0001, ** P =.0025 for RhoGDI1 KO clone #2 (**J**), (one-way ANOVA test; n=40 cells and m=2 experiments).

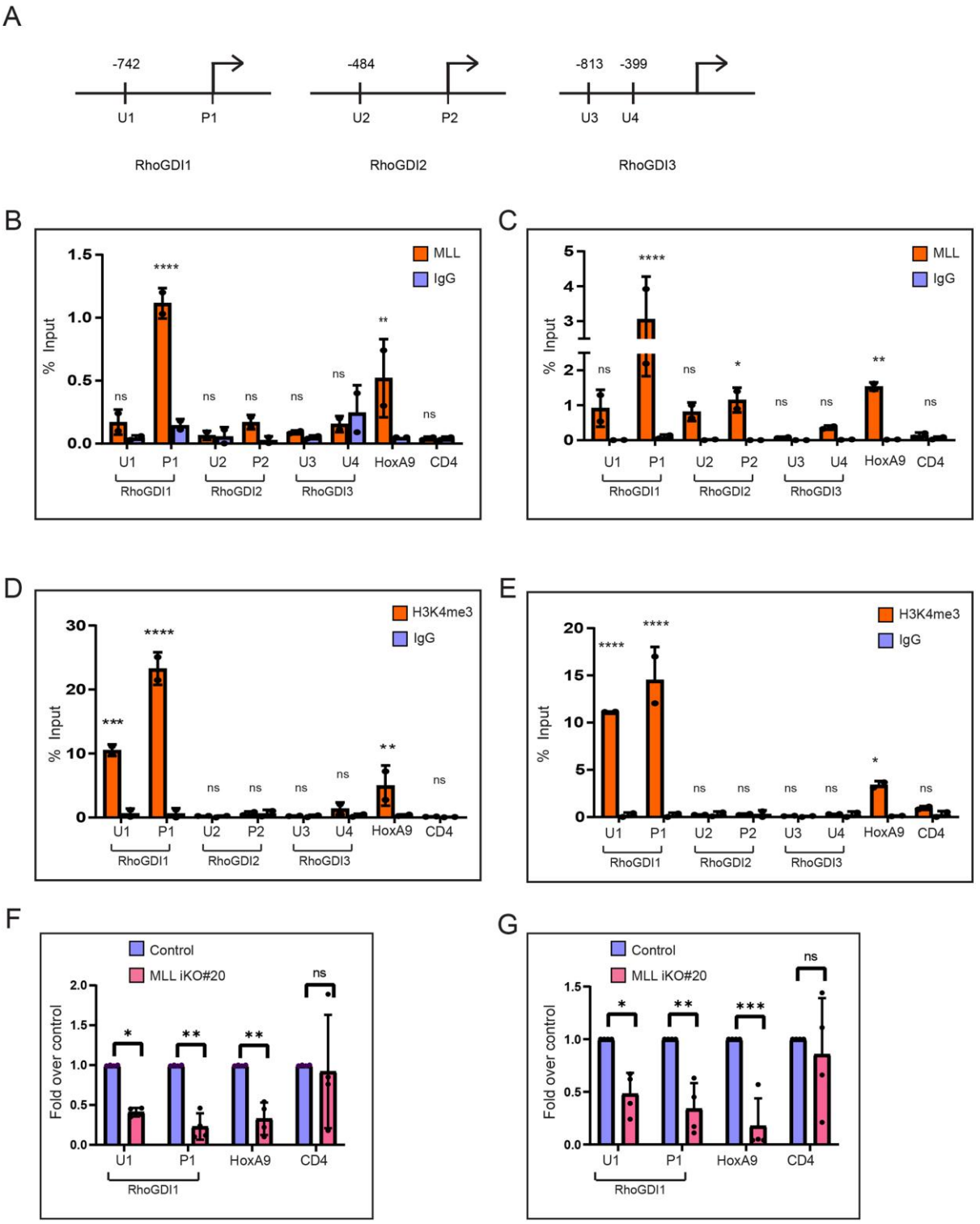

Fig. 6. MLL binds to RhoGDI1 promoter to deposit H3K4 trimethylation mark.

(A) Schematic of regions of genes, where the primers for chromatin immunoprecipitation (ChIP) assay were designed, is shown. Primers in promoter region are denoted by 'P' and upstream region by 'U'. Considering the transcription start site as +1, the exact base position of the respective upstream primers are indicated. (**B**,**C**) ChIP assay was performed using anti-

MLL and IgG antibodies in IMR-90tert **(B)** and HEK-293T cell lines **(C)** Primers used, are indicated in the graphs. (**D**,**E**) ChIP assay was performed using H3K4me3 and IgG antibodies in IMR-90tert **(D)** and HEK-293T cell lines **(E)**. (**F**, **G**) ChIP assay was performed using anti-MLL antibody (**F**) and anti-H3K4me3 antibody (**G**) in HEK-293 control (Cas-9 expressing) and MLL KO clone #20 cell lines. The immunoprecipitated DNA was quantified with RT-qPCR and the results are plotted as percent input enrichment. The error bars represent mean ± S.D. two-way ANOVA, *P ≤.05, **P ≤.01, *** P ≤.001, ****P ≤.0001, ns: not significant, P >.05. All the experiments are done at least twice.

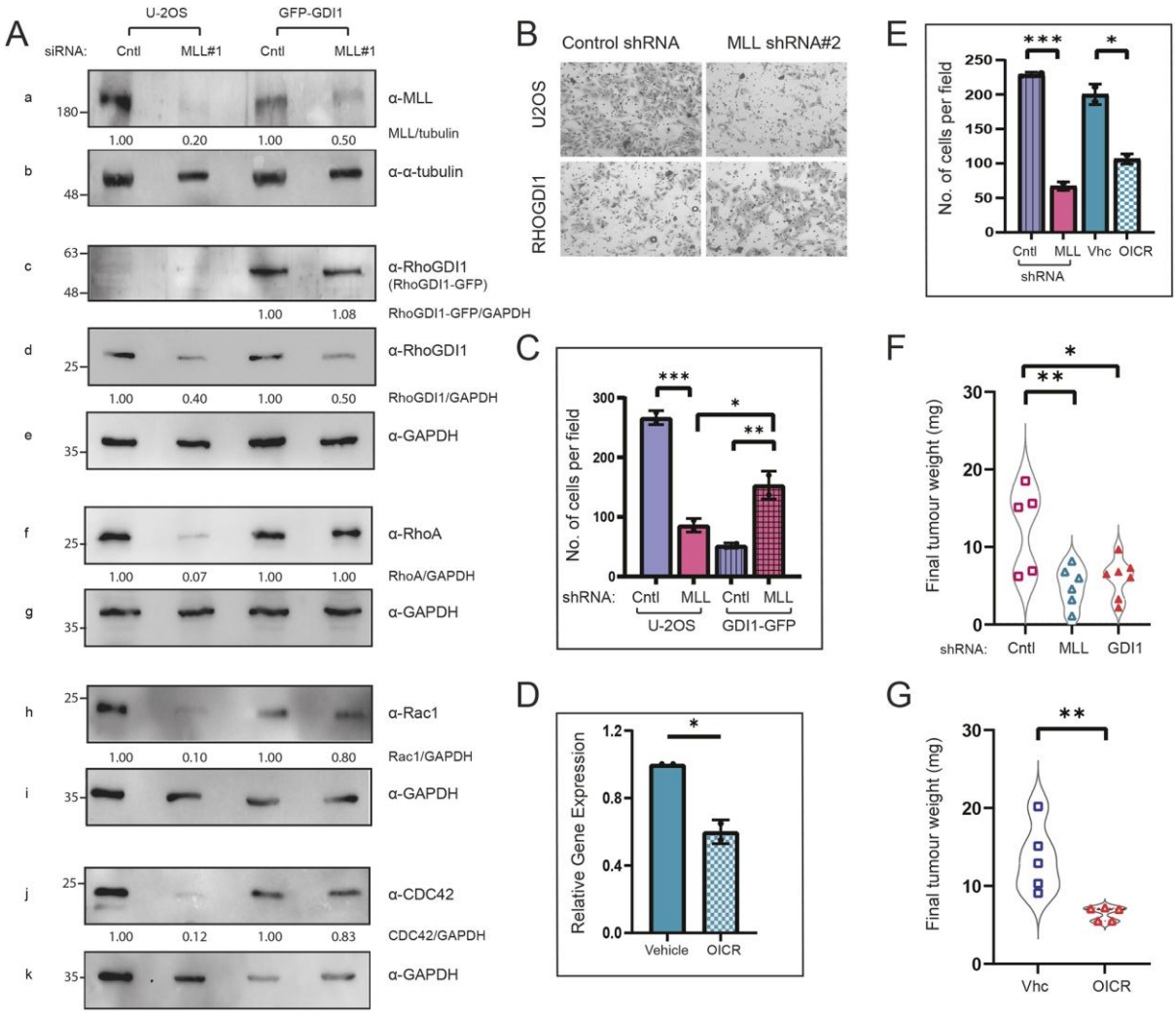

Fig. 7. Exogenous expression of RhoGDI1 can rescue some phenotype associated with loss of MLL.

(**A**) Western blot analysis of whole cell lysates from U-2OS cells as well as GFP-RhoGDI1 cell line, treated with control and MLL siRNA#1 for 72 hr., is shown. The immunoblots were probed with indicated antibodies. (**B**) Wild type U-2OS cells and GFP-RhoGDI1 expressing cells were treated with control and MLL shRNA#2, and seeded for transwell migration assay. Bright field images for migrated cells were captured at 10x magnification. (**C**) Quantifications for number of cells migrated in **(B)** is shown. Data represents mean ± SD, *** P <.001, * P = .0214 and **P =.005 (one-way ANOVA test; m=2 experiments). **(D)** Shown is RT-qPCR analysis of gene expression of RhoGDI1 in MDA-MB-231 cells upon treatment with 25μM OICR-9429. Data represents mean ± SD, *P = .0323 (Student's unpaired t-test; m=2 experiments). (**E**) MDA-MB-231 cells were treated with control or MLL#2 shRNA for 48 hr., or vehicle (DMSO) or 25 μM OICR-9429 for 72 hr., used for

transwell migration assay and number of migrated cells were quantified. Data represents mean ± SD, *** P = .0008, * P = .0153 (Student's unpaired t-test; m=2 experiments). **(F)** Tumours obtained from xenografts of–MDA-MB-231 cells, treated with control, MLL shRNA #2 or RhoGDI1 shRNA #2 were harvested, weighed and plotted. ** P =.007, * P = .014 one-way ANOVA test was performed. (n = 5, 6 and 7 animals for control, MLL and RhoGDI1 shRNA treatment groups respectively) **(G)** Tumours obtained after treatment with vehicle (DMSO) or 4 mg/ Kg OICR-9429, were harvested, weighed and plotted. Data represents violin plot with all data points, ** P =.008, Student's unpaired t-test was performed. (n = 5 animals each). Cntl, control; vhc, vehicle; mg, milligrams; OICR, OICR-9429.

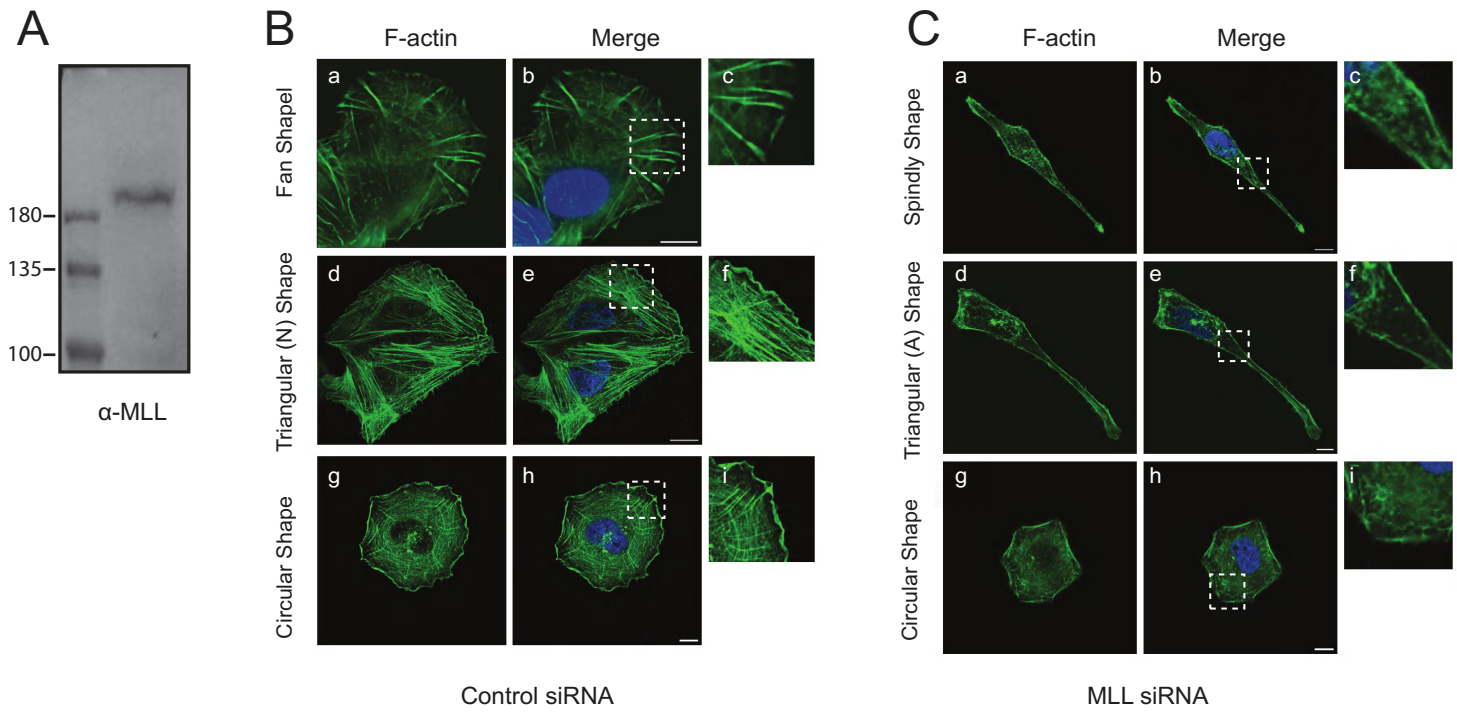

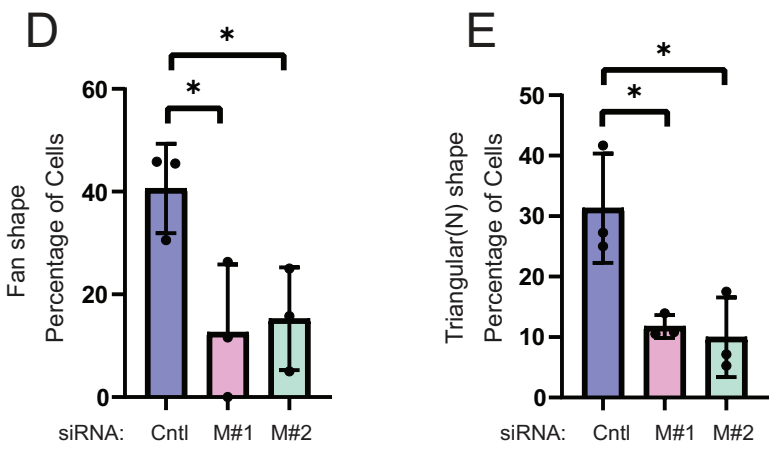

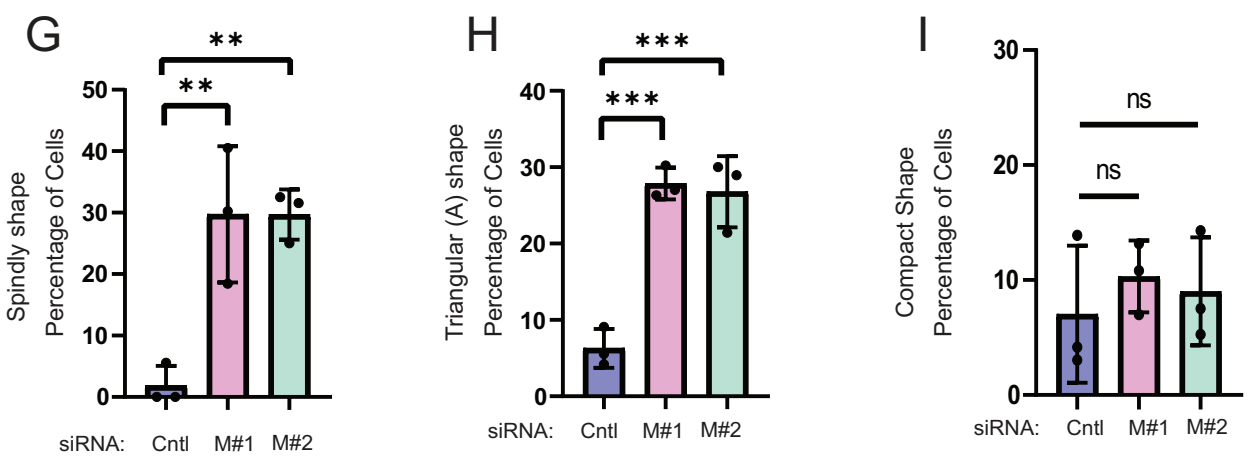

Fig. S1. Loss of MLL affects cell shape and actin cytoskeleton.

(A) U-2OS cells were lysed and immunoblotted. Blot was then probed with in-house generated MLL antibody. Molecular weights are indicated on the left. **(B-C)** U-2OS cells treated with control or MLL siRNA were fixed and used for immunofluorescence and stained with rhodamine conjugated phalloidin to mark filamentous actin (green). Nucleus was stained using 4', 6'-di-amidino 2-phenylindole (DAPI, blue). Representative images from control (**B**) and MLL (**C**) siRNA-treated cells exhibiting three major shapes are displayed, which are quantified in Figure **1D** as well as here. Images from individual MLL siRNA treatment are shown in Figure **1C**. White box indicates region shown in inset. Scale bar, 10 μm. **(D-I)** Quantification of percentage of cells showing different cell shapes from **B-C**. Data represents mean ± SD. *P = .0339 and .0493 **(D)**, *P = .0188 and .0128 **(E)**, ns P = .5140 and .8304 **(F)**, **P = .0052 each **(G)**, *** P = .0004 and .0005 **(H)**, ns P =.6284 and .8323 **(I)** for M#1 and M#2 respectively. F-actin, filamentous-actin; Cntl, control; M#1, MLL siRNA1; M#2, MLL siRNA#2; Triangular (N), Triangular (Normal); Triangular (A), Triangular (Abnormal).

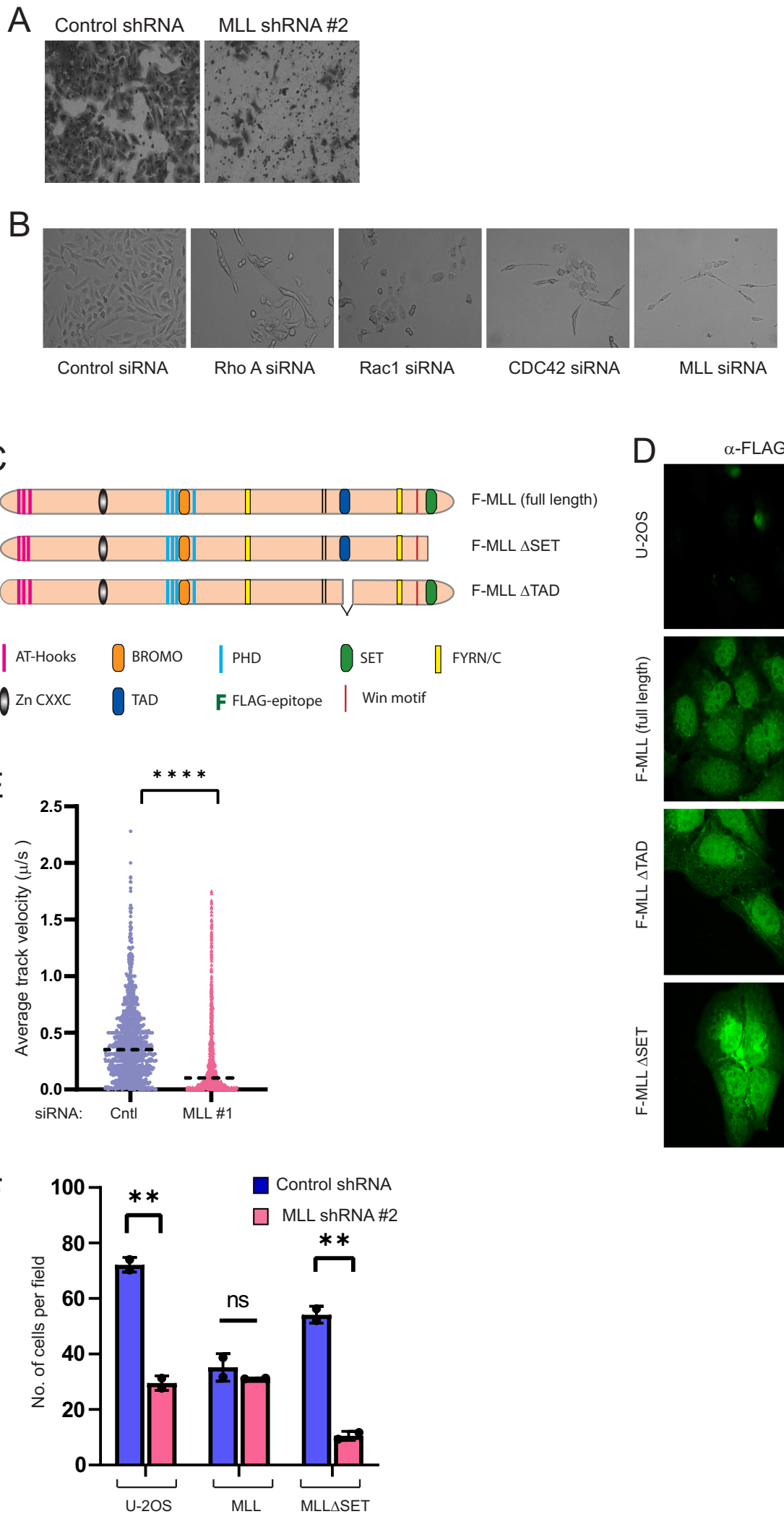

Fig. S2. Depletion of MLL alters cell-spreading and cell migration.

(A) U-2OS cells were treated with control or MLL shRNA#2 for 48 hr. and transwell migration (Boyden chamber) assay was performed. Bright field images show migrated cells upon treatment with respective shRNAs as indicated. (**B**) Bright field images of U-2OS cells treated with various siRNAs (indicated below the images) for 72 hr. Images were captured in Zeiss Axiovert 40 CFL at 10X magnification. (**C**) Schematic of domain architecture of FLAG epitope tagged full length MLL and its different mutants used for the rescue experiments is shown. F-MLL (full length) denotes FLAG epitope tagged MLL protein with all its domains intact whereas F-MLLΔSET and ΔTAD denote recombinant MLL protein devoid of its transcription effector— SET or transactivation —domain respectively. Domains of MLL which impart it chromatin binding capabilities are shown as indicated: AT hooks bind to minor grove of DNA, Zinc finger (Zn) CXXC domain helps in recognition of unmethylated CpG islands, Bromodomains (Bromo) are essential for protein-protein interactions, plant homeodomain (PHD) of MLL help it to read histone marks. The 'FY' rich N-terminal (FYRN) and 'FY' rich C-terminal (FYRC) domains are required for hetrodimerization of MLL_N with MLL_C subunits. WDR5 interacting (Win) motif is responsible for interacting with WDR5. (**D**) U-2OS and U- 2OS cells expressing full length MLL and its various mutants tagged with FLAG epitope tag were fixed for immunofluorescence. Cells were stained with anti-FLAG antibody (green) to detect recombinant MLL expression and nucleus was stained with DAPI. Scale bar, 10 µm. (**E**) Average track velocities from time-lapse images in Figure **3G** are shown. ****P <.0001, (Student's unpaired t test; n = 44 movies for each siRNA from 3 experiments). **(F)** U-2OS cells and U-2OS expressing various mutants of MLL were treated with control and MLL shRNA#2 for 48 hours and 10^5 cells were seeded for transwell migration assay. Quantifications for number of cells migrated per field of image is shown. Data are represented as mean ± SD. **P =.004 (U-2OS) and .003 (SET) ns, P = .4 respectively (Student's unpaired t test, m=2 experiments). ns, non-significant; cntl, control.

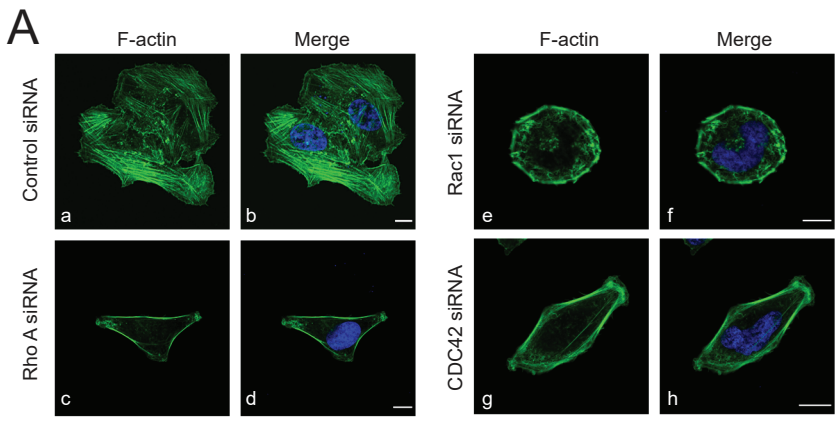

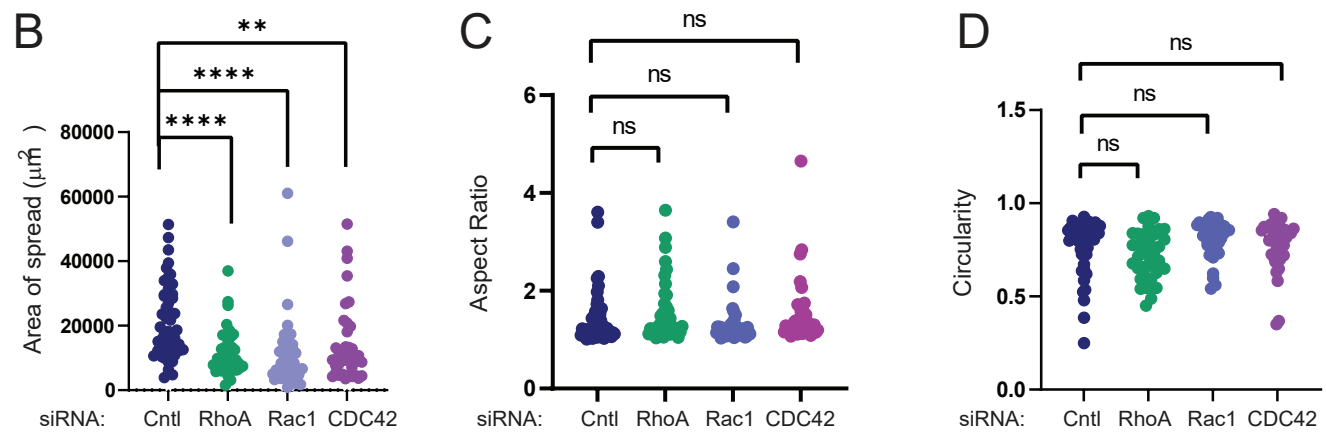

Fig. S3. Rho GTPases depletion alters cell-spreading.

(**A**) Fibronectin spreading of control U-2OS cells (panels a and b) and U-2OS cells upon knock down of Rho GTPases: RhoA (panels c and d), RAC1 (panels e and f) and CDC42 (panels g and h). The cells were stained with rhodamine-conjugated phalloidin to mark F-actin (green) and DAPI to mark nucleus (blue). Scale bar, 10 μm. (**B**) Quantification of area of spread of cells treated with respective siRNAs. Data represents violin plot with all the data points. ***P =.0005 for RhoA siRNA, ****P <.0001 for RAC1 siRNA and **P =.001 for CDC42 siRNA-treated cells respectively. (**C**) Quantification of aspect ratio of cells treated with respective siRNAs. Data represents violin plot with all the data points. ns, P =.72, .62, .90 for RhoA, RAC1 and CDC42 siRNA treated cells respectively. (**D**) Quantification of circularity of cells treated with respective siRNAs. Data represents violin plot with all the data points. ns, P =.09, .22, .99 for RhoA, RAC1 and CDC42 siRNA treated cells respectively. (**B-D**) One-way ANOVA test. n = 40 cells and m = 2 experiments. F-actin, filamentous actin; Cntl, control. ns, non-significant.

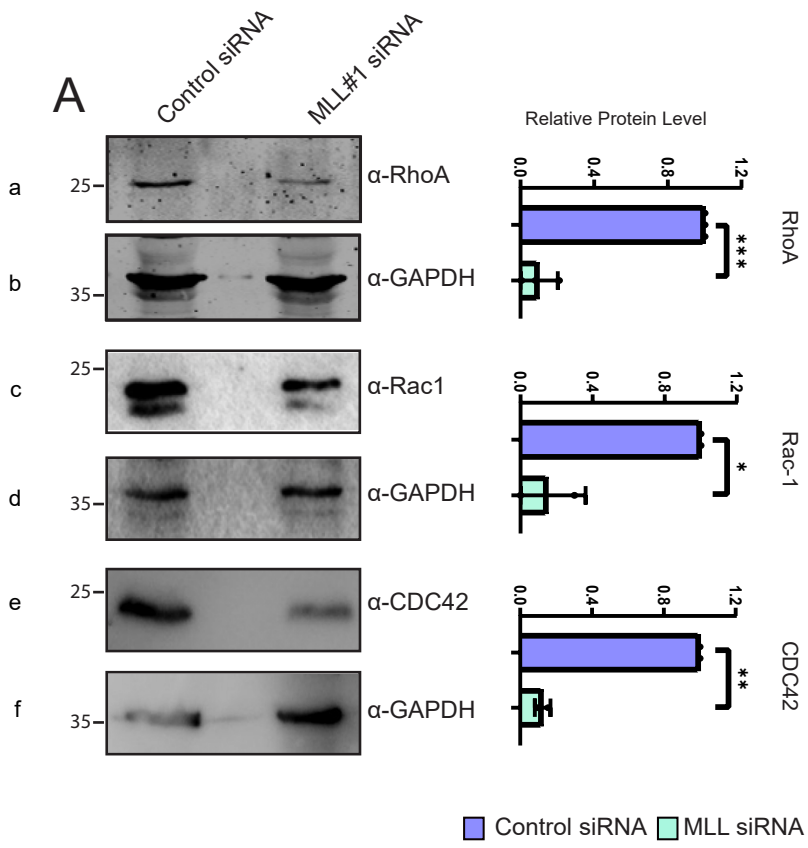

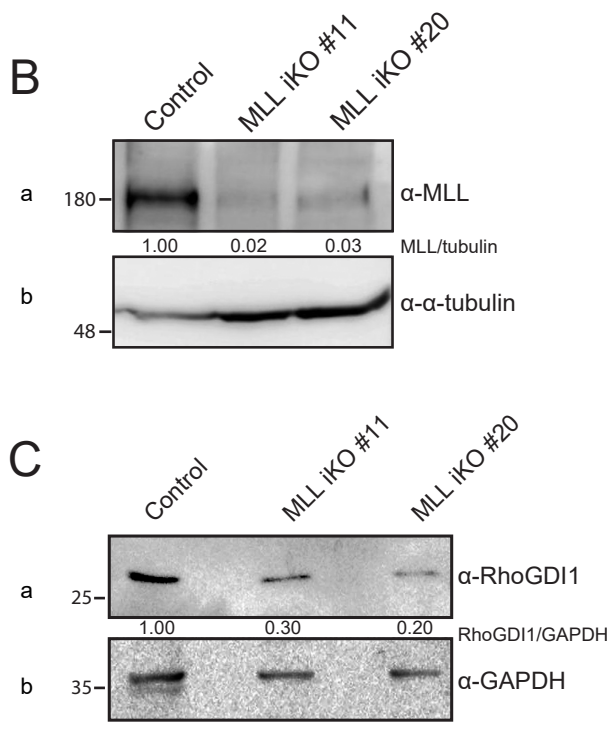

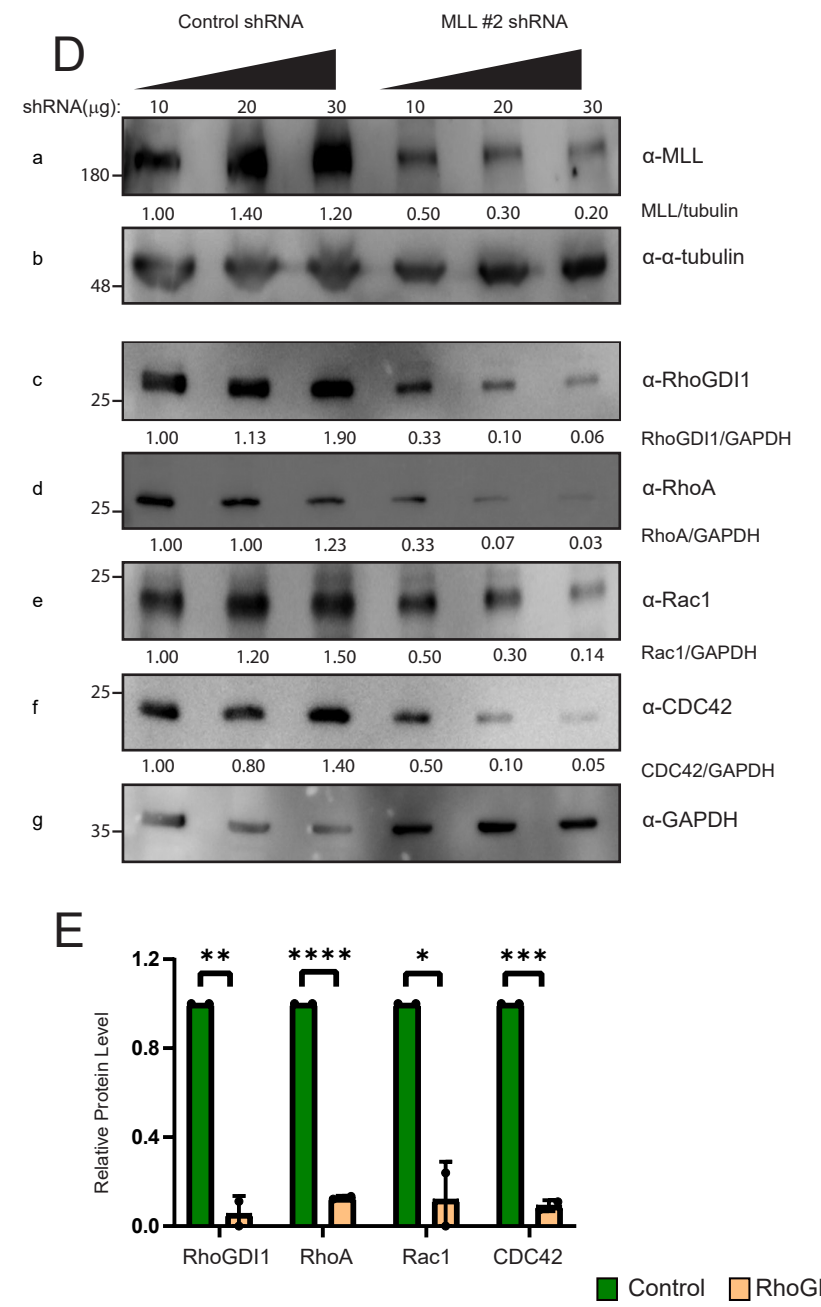

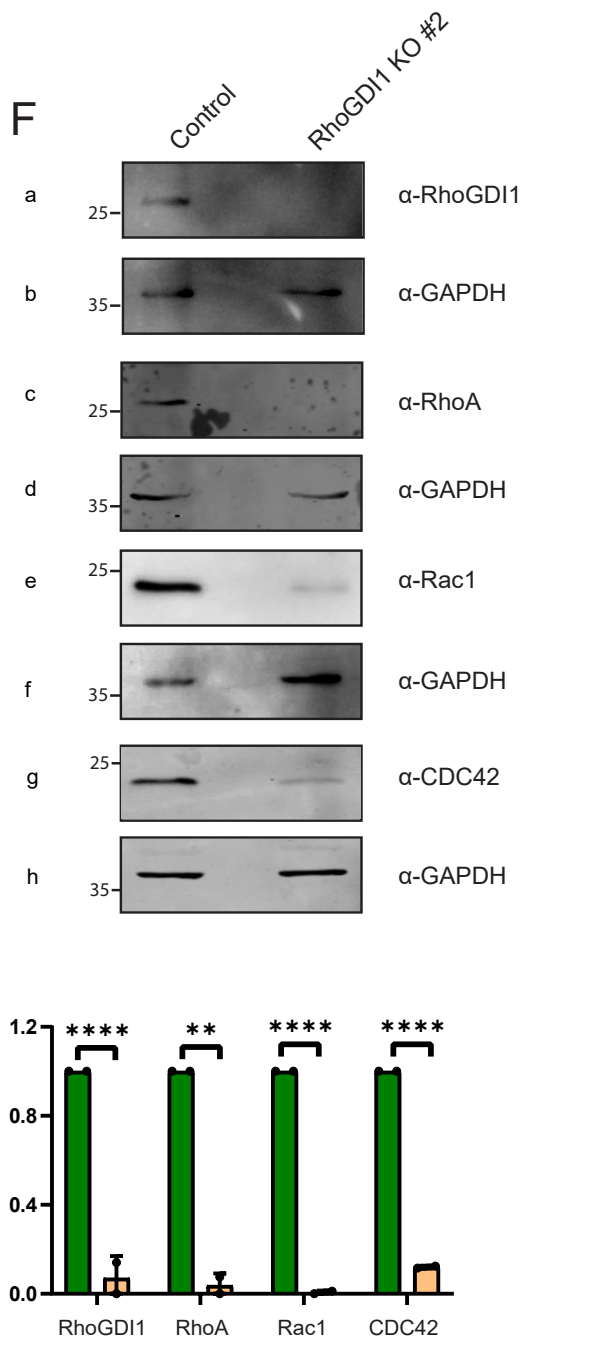

Chinchole Supplementary Figure 4

Fig. S4. MLL regulates the protein levels of RhoGDI1.

(A) MDA-MB-231 cells treated with either control or MLL#1 siRNA, were harvested after 72 hr., lysed and immunoblotted. The blots were probed with various antibodies as indicated on the right. Panels a, c and e show the endogenous protein levels of RhoA, Rac1 and CDC42 respectively upon MLL depletion. Panels b, d and f indicate loading control, GAPDH. Numbers on the left indicate molecular weight markers in kDa. Quantifications of protein levels relative to loading control are shown on the right of the blots. Data represents mean ± SD. ***P = .0001, *P = .0296 and ** P = .0012 for RhoA, Rac1 and CDC42 respectively. (Student's unpaired t test, m=2 experiments). (B, C) Control HEK-293 and MLL knock out cell lines #11 and #20 were lysed in NETN buffer and immunoblotted. The blots were probed with MLL antibody (B, panel a), RhoGDI1 antibody (C panel a), and loading control, -tubulin (B panel b) and GAPDH (C, panel b). (D) U-2OS cells treated with 10, 20 or 30 µg of control or MLL shRNA#2 were lysed and immunoblotted. Blots were probed with anti-MLL, RhoGDI1, RhoA, Rac1 and CDC42 antibodies as indicated. Loading control, -tubulin and GAPDH are indicated in panels b and g respectively. (E) Quantification of protein levels relative to loading control of immunoblots from Figure 5E are shown. Data represents mean ± SD. **P = .0035, ****P <.0001, *P = .018, ***P= .0004. Student's unpaired t-test, m= 2. (F) Control U-2OS and RhoGDI1 knock out #2 cells were lysed and immunoblotted. The blots were probed with anti RhoGDI1 (panel a), RhoA (panel c), RAC1 (panel e) and CDC42 (panel g) antibodies respectively. Loading control, GAPDH is shown in panels b, d, f and h for respective blots. (G) Quantification of relative protein levels from immunoblots in F are shown. Data represents mean ± SD. ****P <.0001 for RhoGDI1, Rac1 and CDC42. **P = .002 for RhoA. Student's unpaired t-test, m= 2. (A-D,F) Numbers on the left indicate molecular weight markers in kDa. KO, knock out.

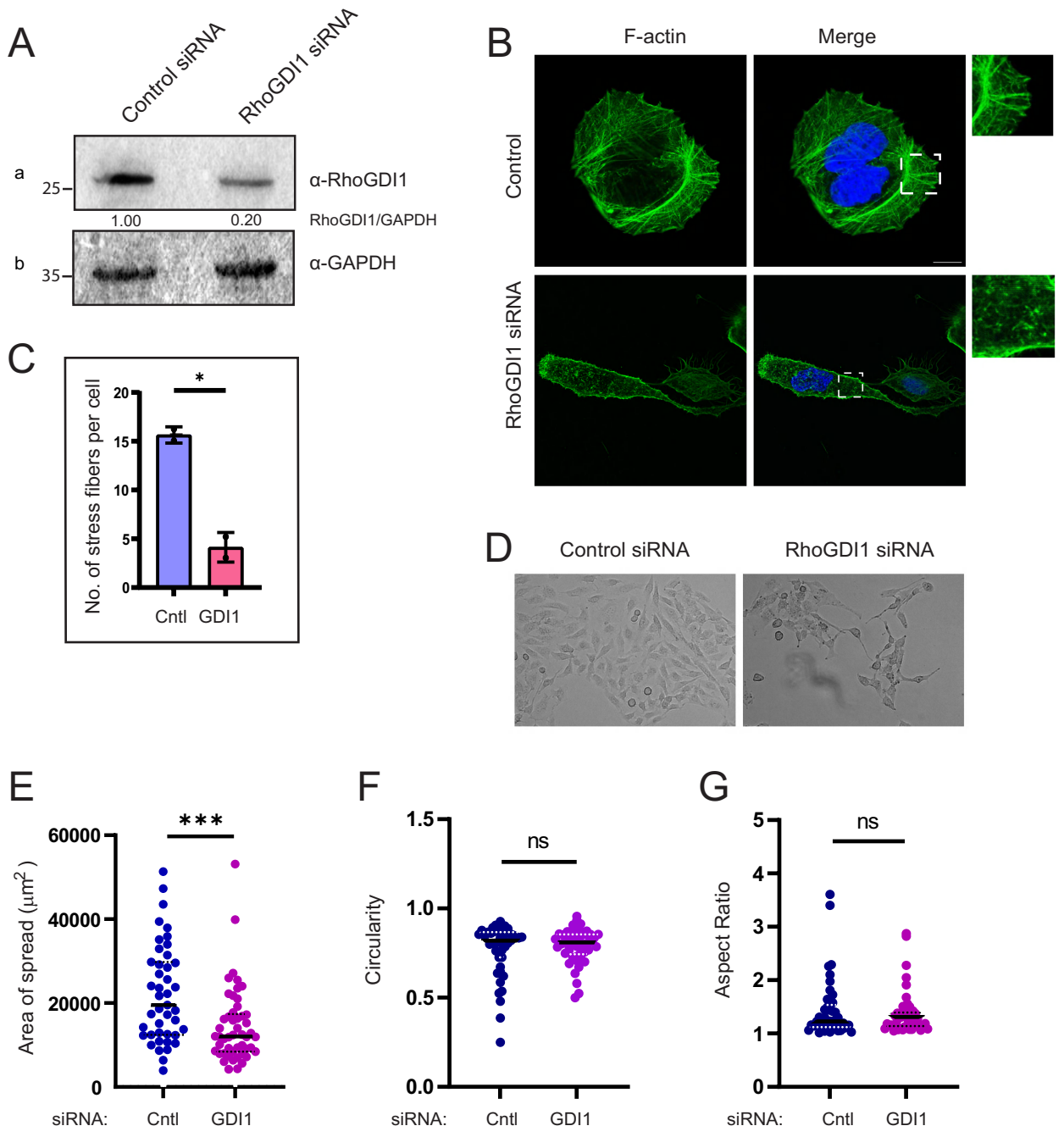

Fig. S5. Depletion of RhoGDI1 affects actin stress fiber formation and cell spreading.

(A) U-2OS cells were treated with control and RhoGDI1 siRNA for 72 hr., lysed and immunoblotted. Blots were probed with RhoGDI1 (panel a) and GAPDH (panel b) antibodies. Numbers on the left indicate molecular weight markers in kDa. **(B)** U-2OS cells were seeded on cover slips and treated with either control or RhoGDI1 siRNA for 72 hr. prior to fixation for immunofluorescence. Actin stress fibers stained with stained with rhodamine-conjugated phalloidin is shown in control siRNA (upper panel) and RhoGDI1 siRNA (lower panel) treated cells respectively. Insets are shown adjacent to IF images. White squares indicate region highlighted in insets. Scale bar, 10 μm. **(C)** Quantification of number of stress fibers per cell from **B** is shown. Data represents mean ± SD. *P = 0.01 (Student's unpaired t-test; n = 40 cells, m = 2 experiments). Data in wild type U-2OS is same as Figure **3E**, as these experiments were done together. **(D)** U-2OS cells were treated with control and RhoGDI1 siRNA for 72 hr. and bright field images were captured at 10x magnification in Zeiss Axiovert CFL 40 microscope. **(E)** U-2OS cells treated with control and RhoGDI1 siRNA were spread on fibronectin coated cover slips for 4 hr. and the area of spread of the cells was quantified. ***P =.0005. **(F)** Quantification of circularity of control and RhoGDI1 siRNA treated U-2OS cells. ns P =.43. **(G)** Quantification of aspect ratio of control and RhoGDI1 siRNA treated U-2OS cells. ns P =.50 **(E-G)** Data represents violin plot with all data points. Student's unpaired t-test; n = 40 cells and m = 2 experiments. F-actin, filamentous actin; Cntl, control; GDI1, RhoGDI1; No., number; ns, nonsignificant.

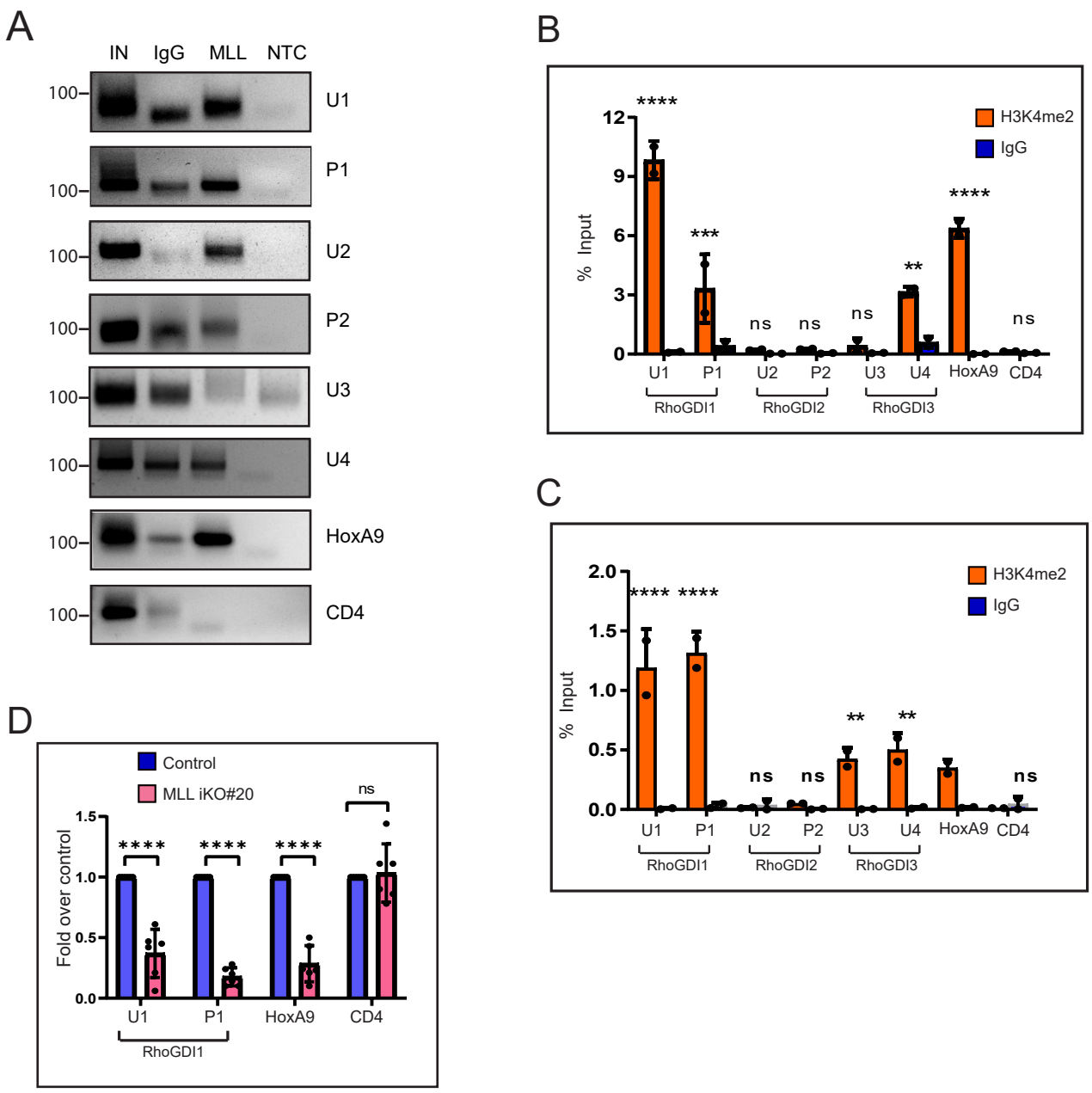

Fig. S6. MLL binds to RhoGDI1 promoter to deposit H3K4 trimethylation marks.

(A) HEK 293 cells were subjected to ChIP PCR analysis using anti-MLL and IgG antibodies. The ChIP samples were subsequently used for RT q-PCR amplification. Agarose gel image of the amplicons obtained from RTq-PCR are shown. Primers used for the amplification are indicated on the right. Numbers indicated on the right are molecular weight marker in base pair. **(B-C)** ChIP was performed cells using H3K4me2 and IgG antibody in IMR-90tert **(B)** and HEK-293T**(C)** cells. (**D**) ChIP assay was performed in HEK-293 control (Cas-9 expressing) and MLL knockout cell lines using H3K4me2 antibody. The immunoprecipitated DNA was quantified as percent input enrichment in **B and C** and as fold change with respect to control in **D,** as described in main text. The antibodies used are indicated in the top right corner of each box. The error bars represent mean ± S.D. two-way ANOVA, *P ≤ .05, **P ≤ .01, *** P ≤ .001, ****P ≤ .0001, ns: not significant, P > 0.05. All the experiments are done at least twice. IN, input; NTC, no template control.

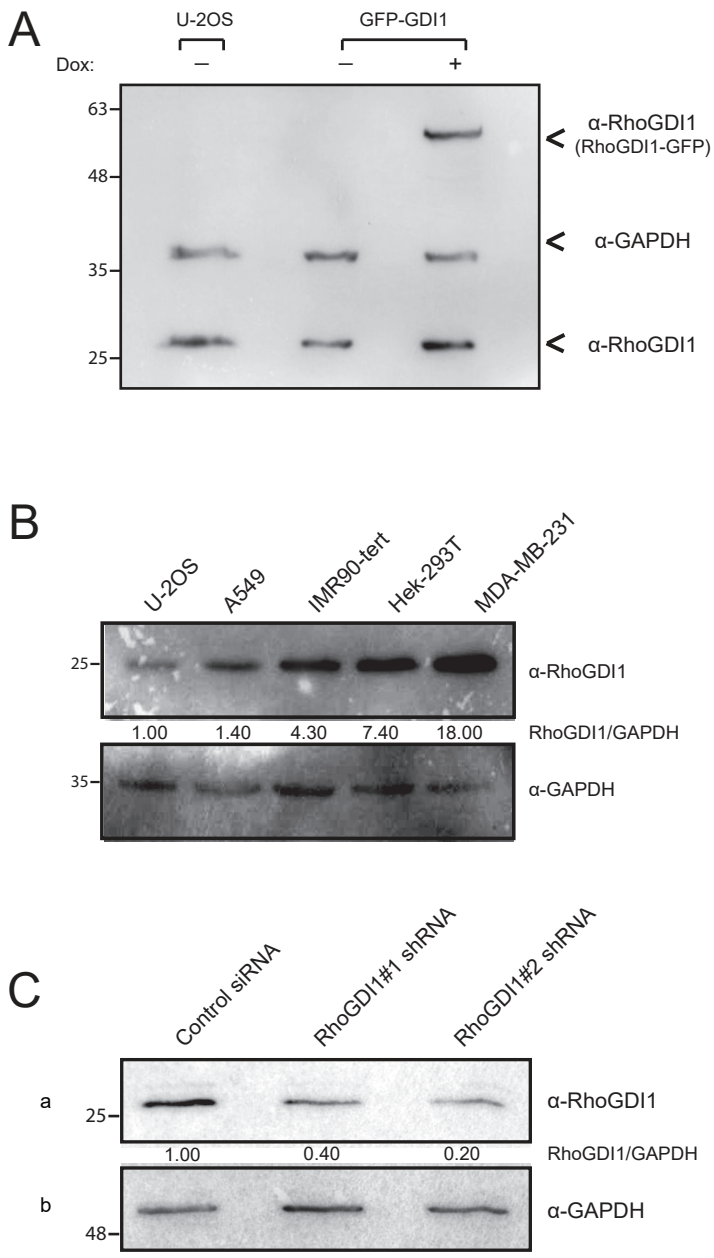

Fig. S7. Endogenous expression of RhoGDI1 in different cell lines.

(A) Western blot analysis of whole cell lysates from U-2OS cells as well as U-2OS cells over-expressing GFP tagged RhoGDI1 (GFP-GDI1) is shown. The expression of GFP-RhoGDI1 is induced by Doxycycline(Dox). The immunoblots were probed with anti-RhoGDI1 antibody (which detected both recombinant RhoGDI1-GFP and endogenous RhoGDI1) and anti-GAPDH antibody is shown. (**B**)Whole cell lysates were prepared from U-2OS, A549, IMR- 90tert, HEK-293T and MDA-MB-231 cell lines and immunoblotted. Blots were probed using RhoGDI1 antibody (upper panel) and GAPDH antibody (lower panel). **(B)** MDA-MB-231 cells were treated with control shRNA or RhoGDI1 shRNA#1 or #2 and incubated for 48 hr. Cells were harvested, lysed and immunoblotted. Blots were probed with RhoGDI1 (panel a) and GAPDH (panel b) antibodies. Numbers indicated on the left are the molecular weight markers.

Supplementary Figure 8 : Blot Trasnparency

Figure 1 A

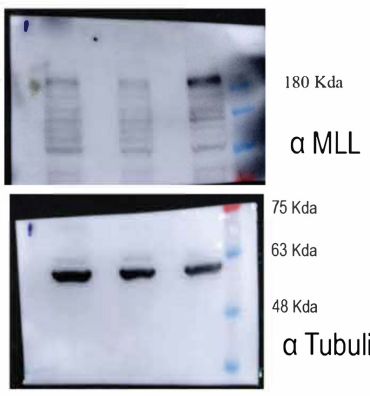

Figure 2 E

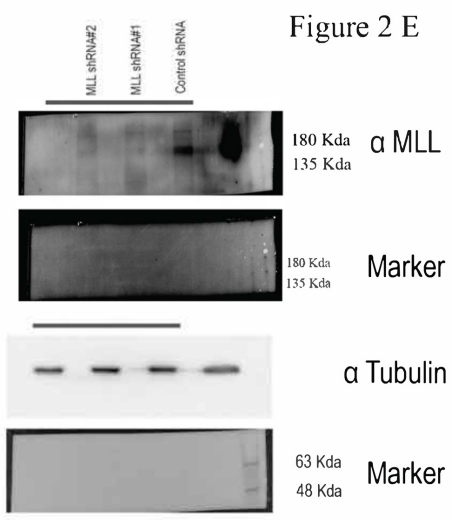

Figure 3A-C

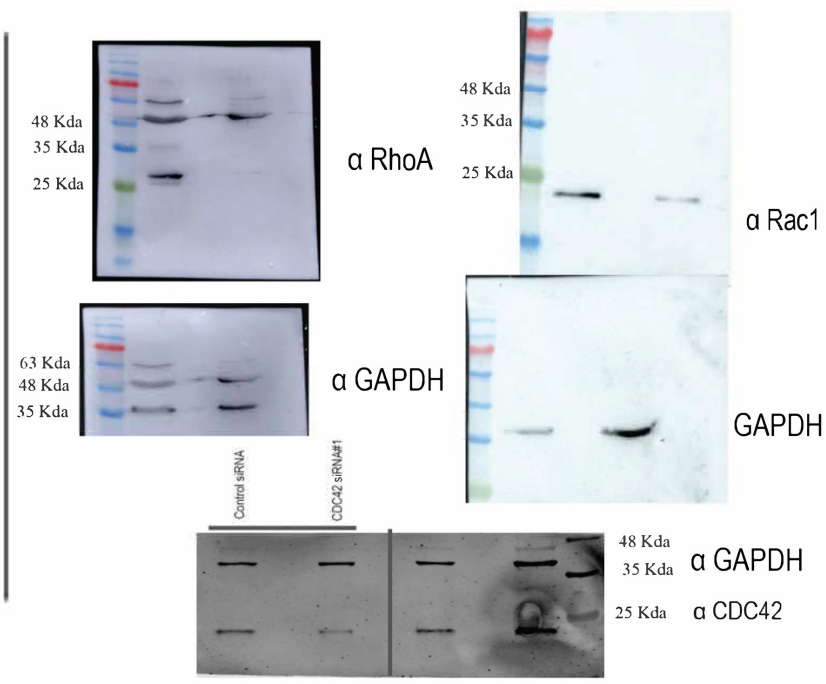

Figure 4A

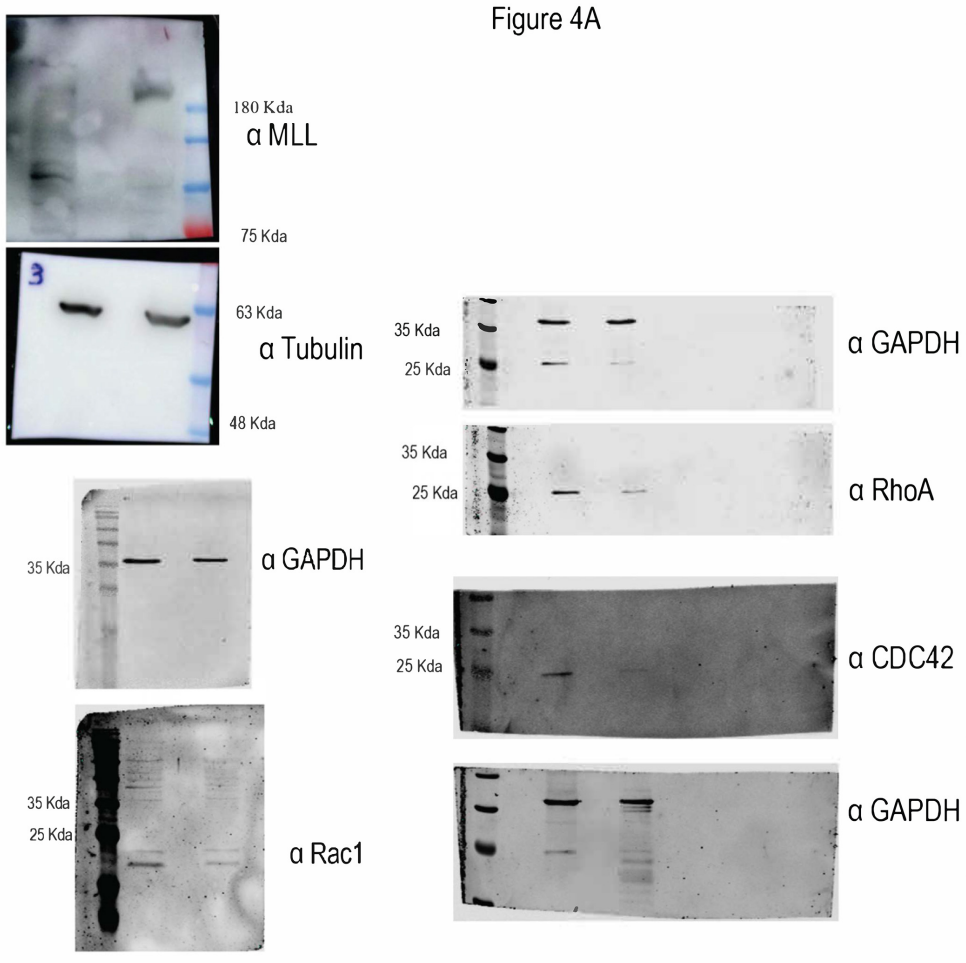

Figure 4B

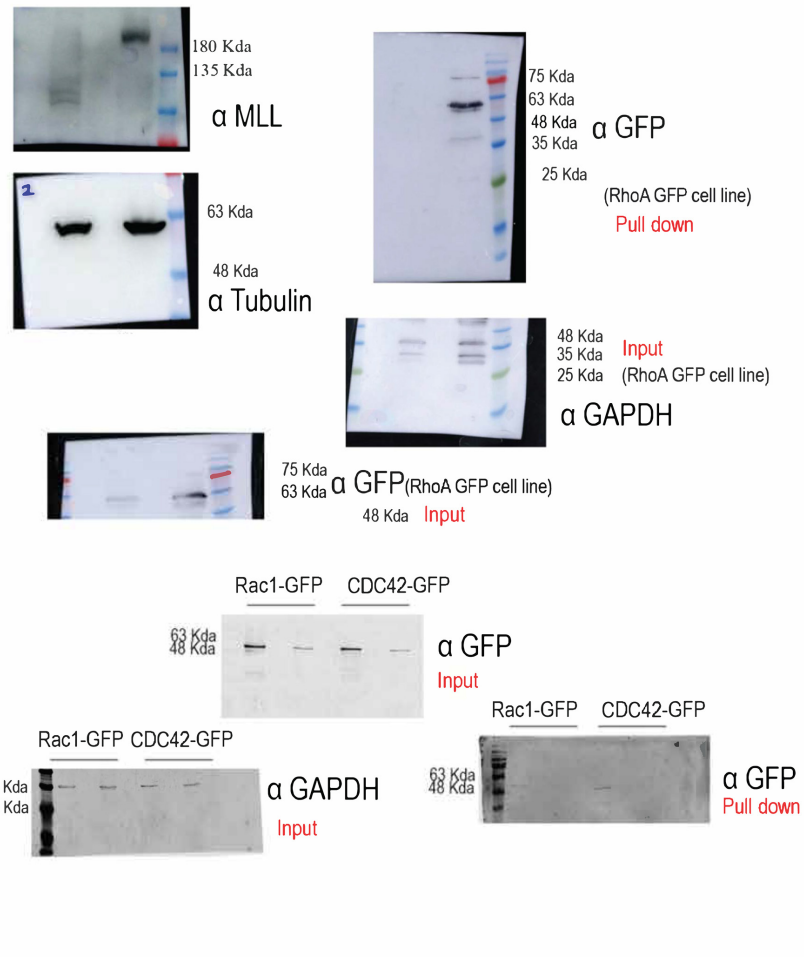

Figure 5A

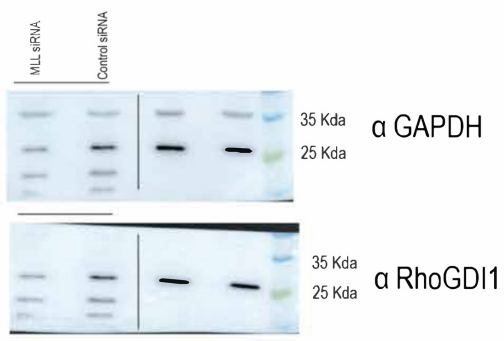

Figure 5B

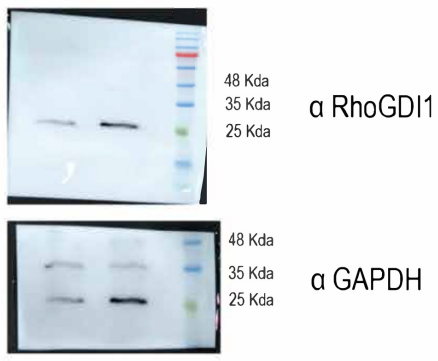

Figure 7A

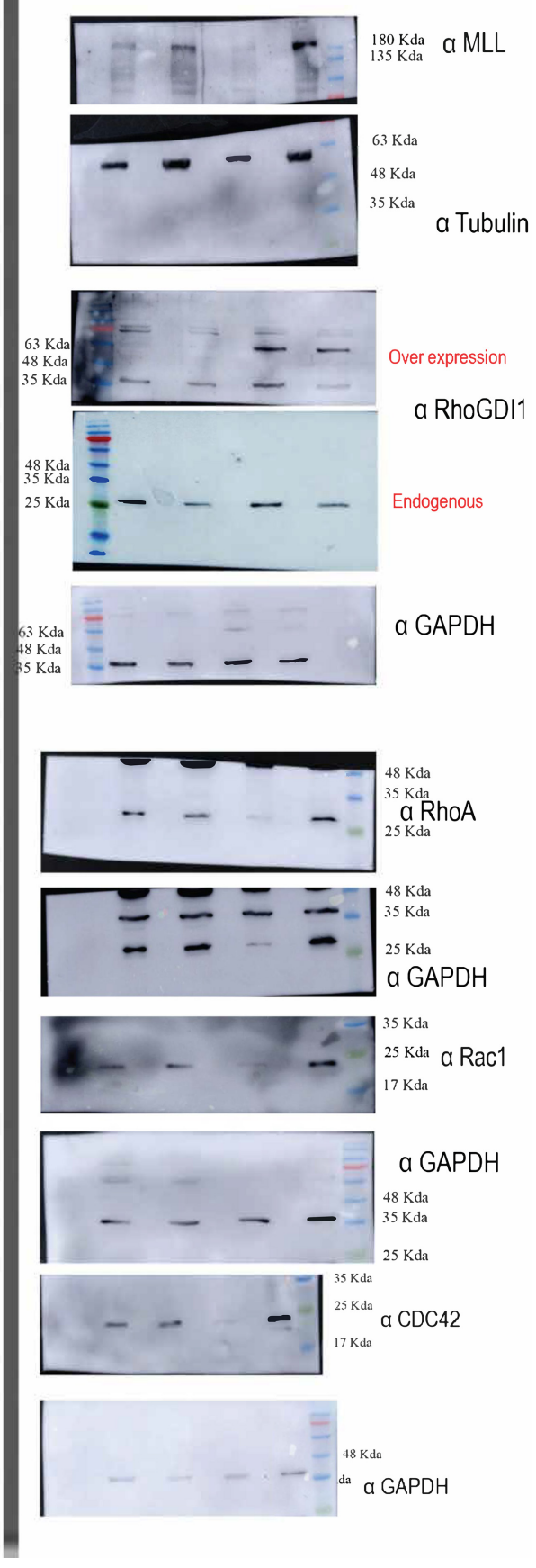

Figure 5E

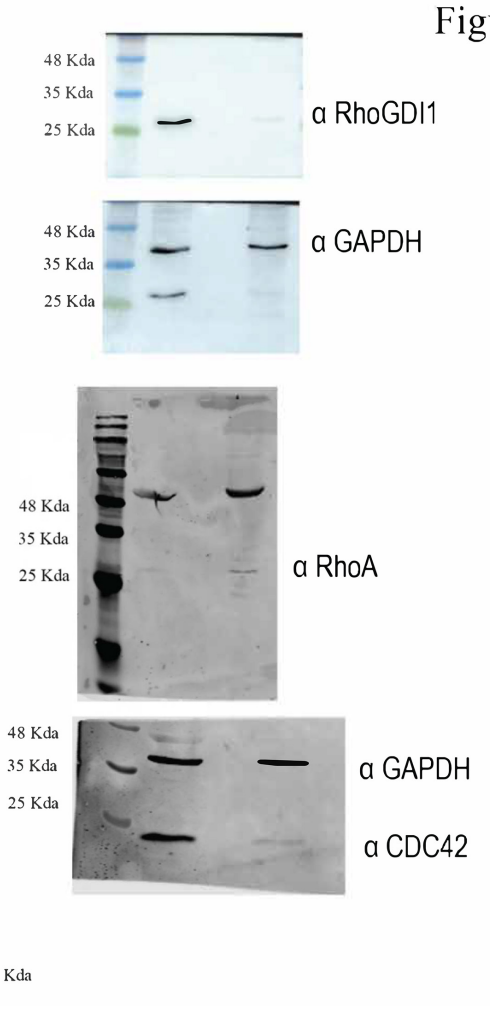

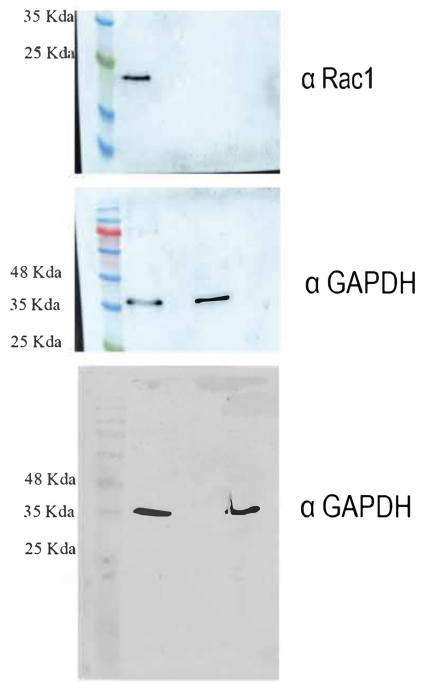

Supplementary Figure 1

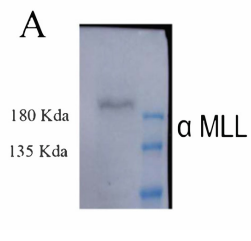

Supplementary Figure 4A

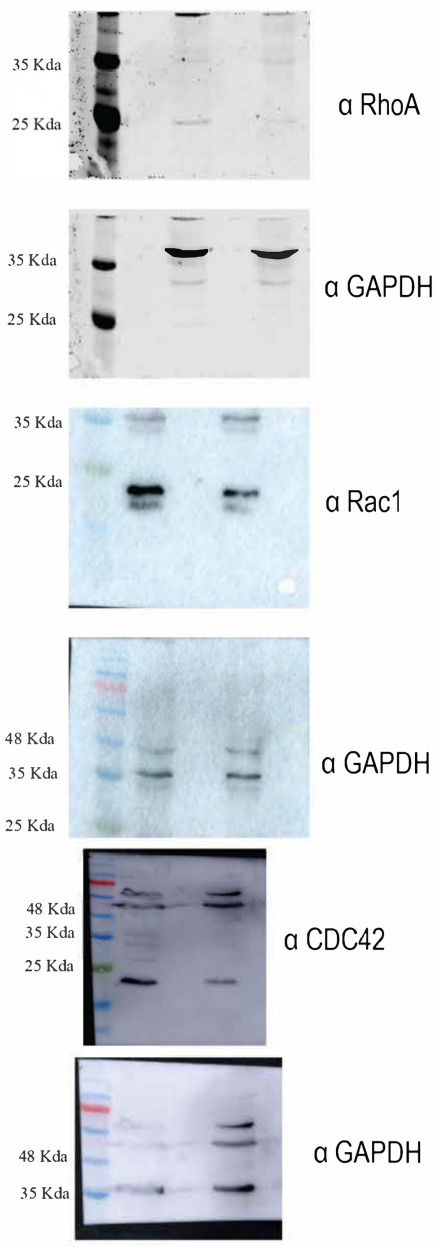

Supplementary Figure 4B

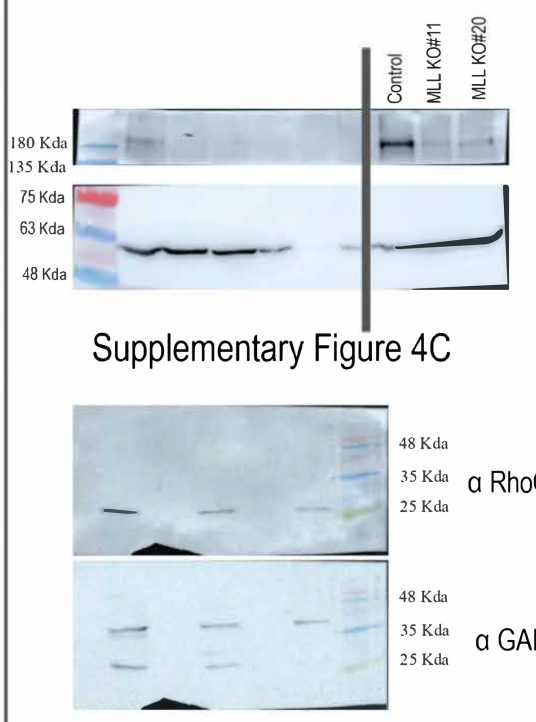

Supplementary Figure 4C

Supplementary Figure 5A

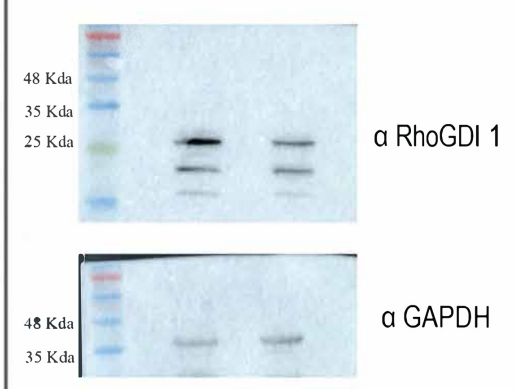

Supplementary Figure 7B

Supplementary Figure 4F

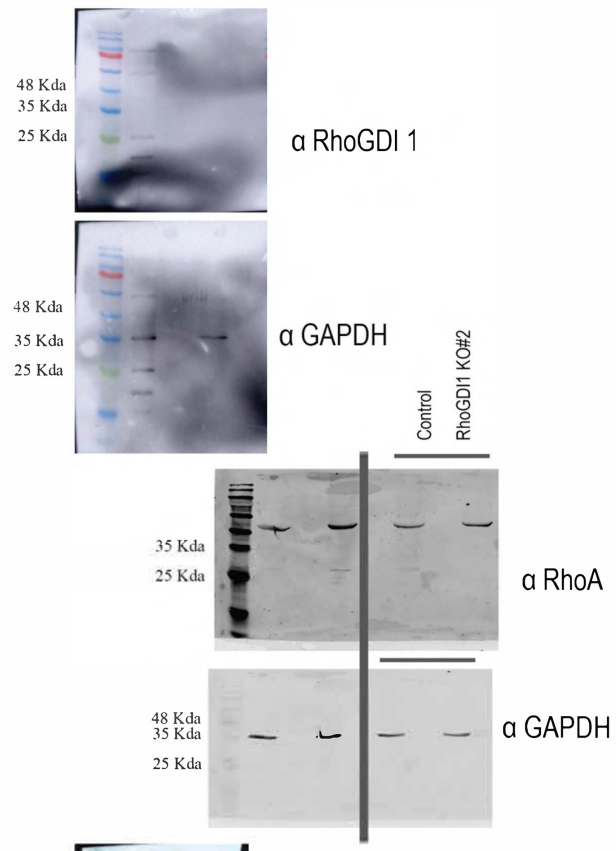

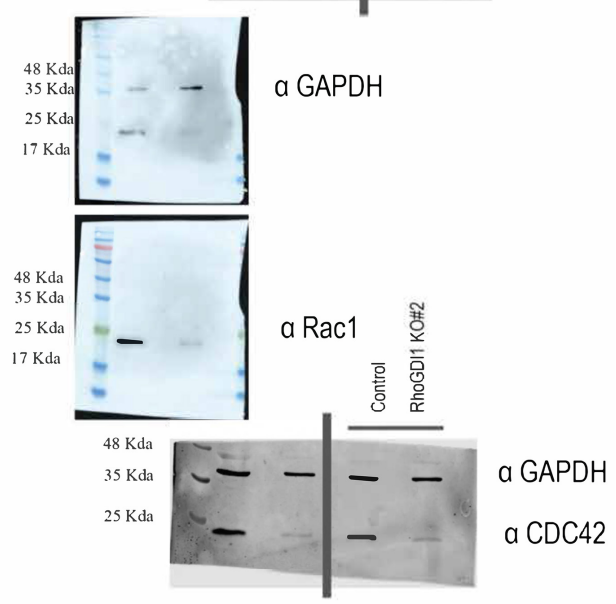

Supplementary Figure 4D

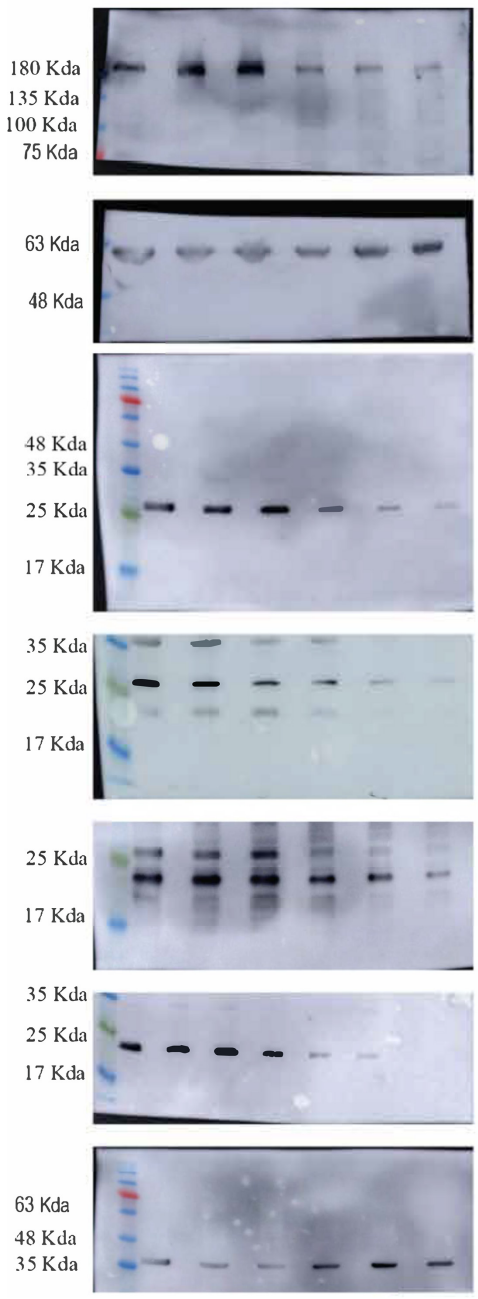

Supplementary Figure 7A

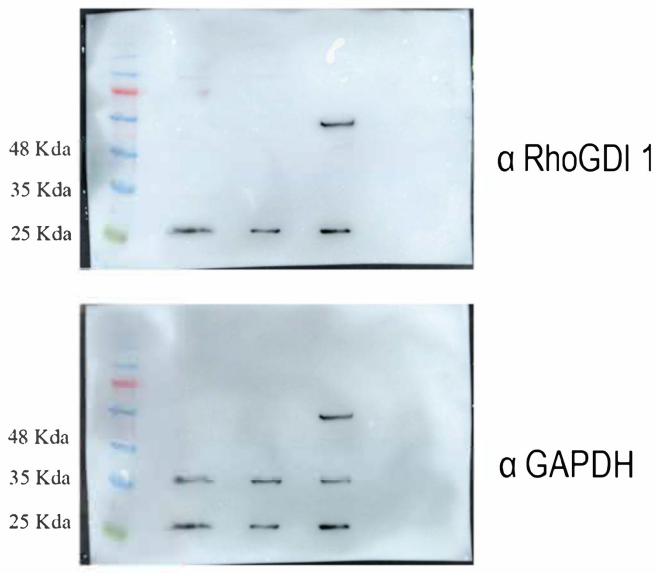

Supplementary Figure 7C

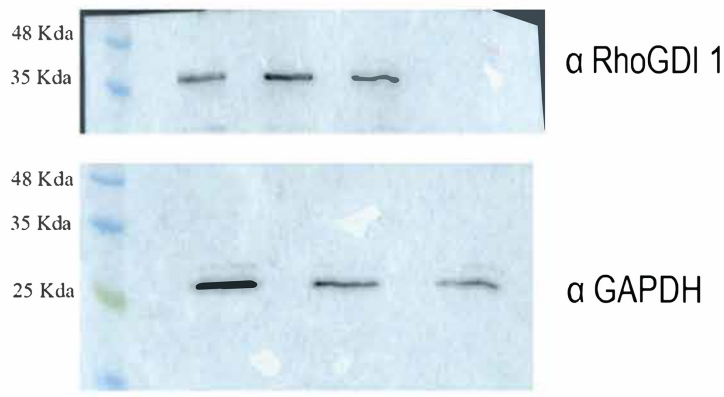

Table S1. Primers used for transcript analysis

Primer Names	Sequences
GAPDH qRT	F: 5'-ATGTTCGTCATGGGTGTGAA-3' R: 5'-GAGGCAGGGATGATGTTCTG-3'
MLL qRT	F: 5'-ATCGTCCACCGCAAATGCTTCTA-3' R: 5'-AGCCATGCCAATCTCATCTTGTT-3'
RhoA qRT	F: 5'-AAGGACCAGTTCCCAGAGGT-3' R: 5'-TTCTGGGGTCCACTTTTCTG-3'
Rac1 qRT	F: 5-'CGCAAACAGATGTGTTCTTA-3' R: 5'-CTAGGATGATGGGAGTGTTG-3'
CDC42 qRT	F: 5'-CTGAAGGCTGTCAAGTATGT-3' R: 5'-GAGAGATGTTCATAGCAGCA-3'
RhoGDI1 qRT	F: 5'-TAGGATCCCGGCGCCTAC-3' R: 5'-TTGGGGTCTGCGGAAACG-3'
RhoGDI2 qRT	F: 5'-ACAAAGCAGGGAAGTGTCAGA-3' R: 5'-GTCAGAGTTGAGAGACAGAGGC-3'
RhoGDI3 qRT	F: 5'-GGACCAGGTGTTTGTCCTGA-3' R: 5'-CCACGGGAGTCACAAACT-3'

Table S2. Primers used for ChIP assay

Primer names	Sequence
RhoGDI1 PROMOTER (P1)	F: 5'-GTGAGCGGAAGTCTCGTG-3' R: 5'-GCCGCGCGGTTCAGGATC-3'
RhoGDI1 UPSTREAM (U1)	F: 5'- GGGCGAATGTGTGGAATCTC-3' R: 5'-CACCGTGAGCAGATGAGGG-3'
RhoGDI2 PROMOTER (P2)	F: 5'-CCAGGGTTTCCTCTTCAAGTAG-3' R: 5'-CTGTCTCTCAACTCTGACTTC-3'
RhoGDI2 UPSTREAM (U2)	F: 5'-GAAGAAAAATCAGCCAAAACTA-3' R: 5'-TCCTTAAACAGATTTTTGGAGT-3'
RhoGDI3 NEGATIVE (U3)	F: 5'-AAGGGCGGGTCTAATTTCTG-3' R: 5'-CTGCGTCTGGATAAGGGAG-3'
RhoGDI3 POSITIVE (U4)	F: 5'-TACTGATGACCGTGAACCTG-3' R: 5'-CTGAGGGAGCTTCTGTCTG-3'
HOXA9	F: 5'-CTCCGCCGCTCTCATTCTCAG-3' R: 5'-GCCAGAAGGGGTGACTGTCC-3'
CD4	F: 5'-TGTGCTCTGCCCAGTTGTCT-3' R: 5'-GCTCATGACCAGTTCCAAGAGAA-3'

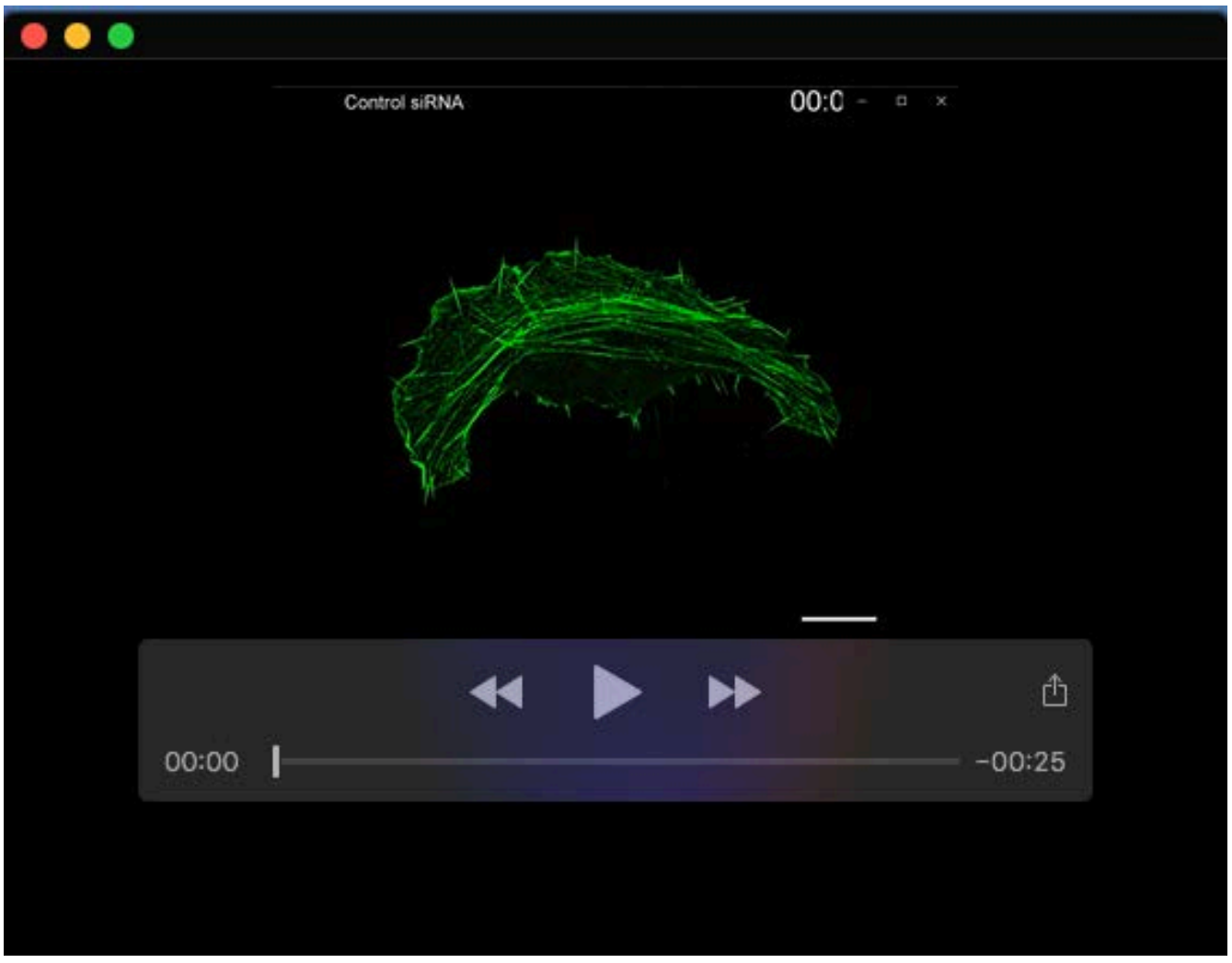

Movie 1. U-2OS cell expressing GFP-Lifeact (green) treated with control siRNA, corresponding to Figure 3G panel a, is shown here. Frame size is 73x73 µm and frame step is 5 s. Scale bar, 10 µm.

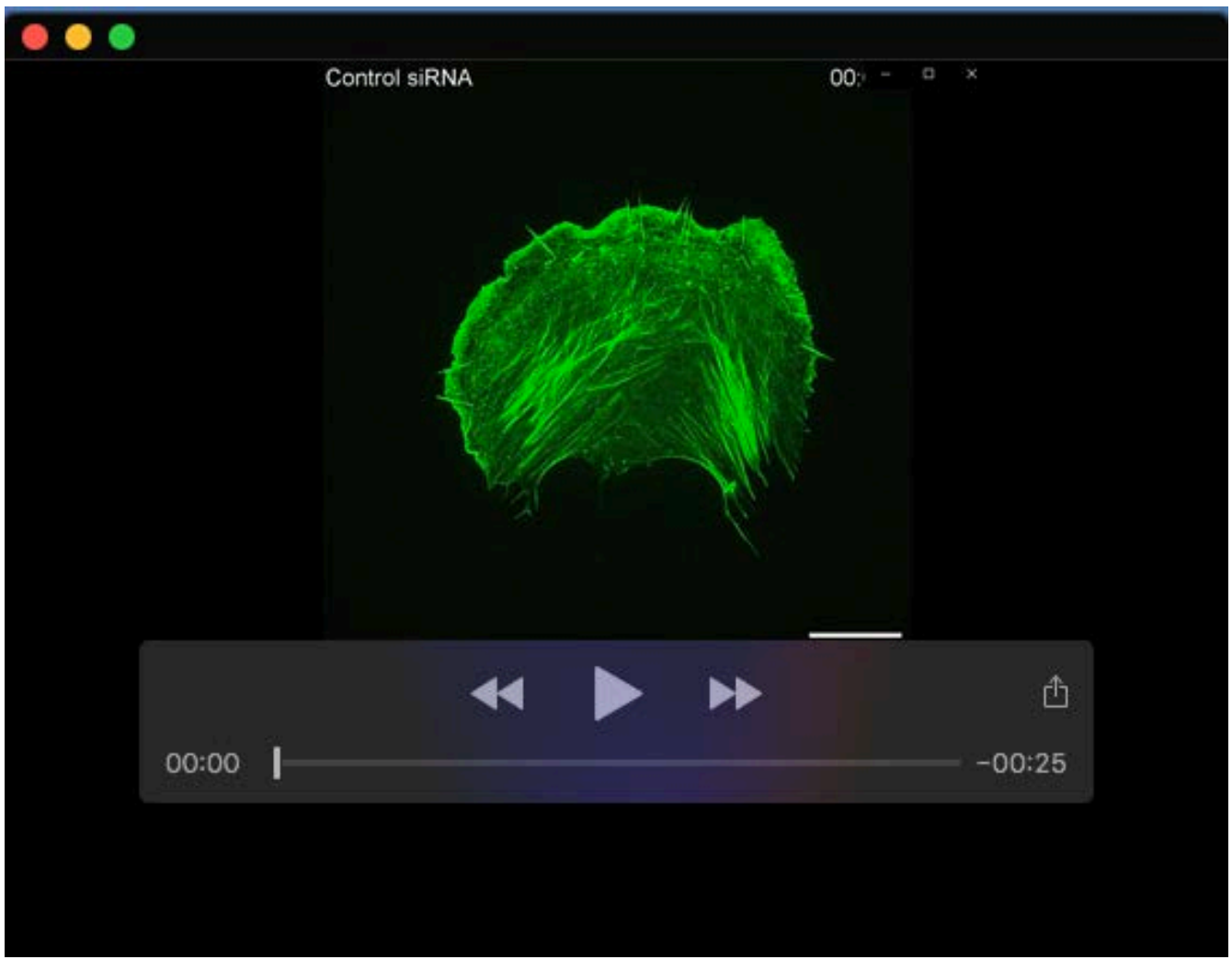

Movie 2.Shown here is U-2OS cell expressing GFP-Lifeact treated with control siRNA, corresponding to Figure 3G panel b, Frame size is 64x64 µm and frame step is 5 s. Scale bar, 10 µm.

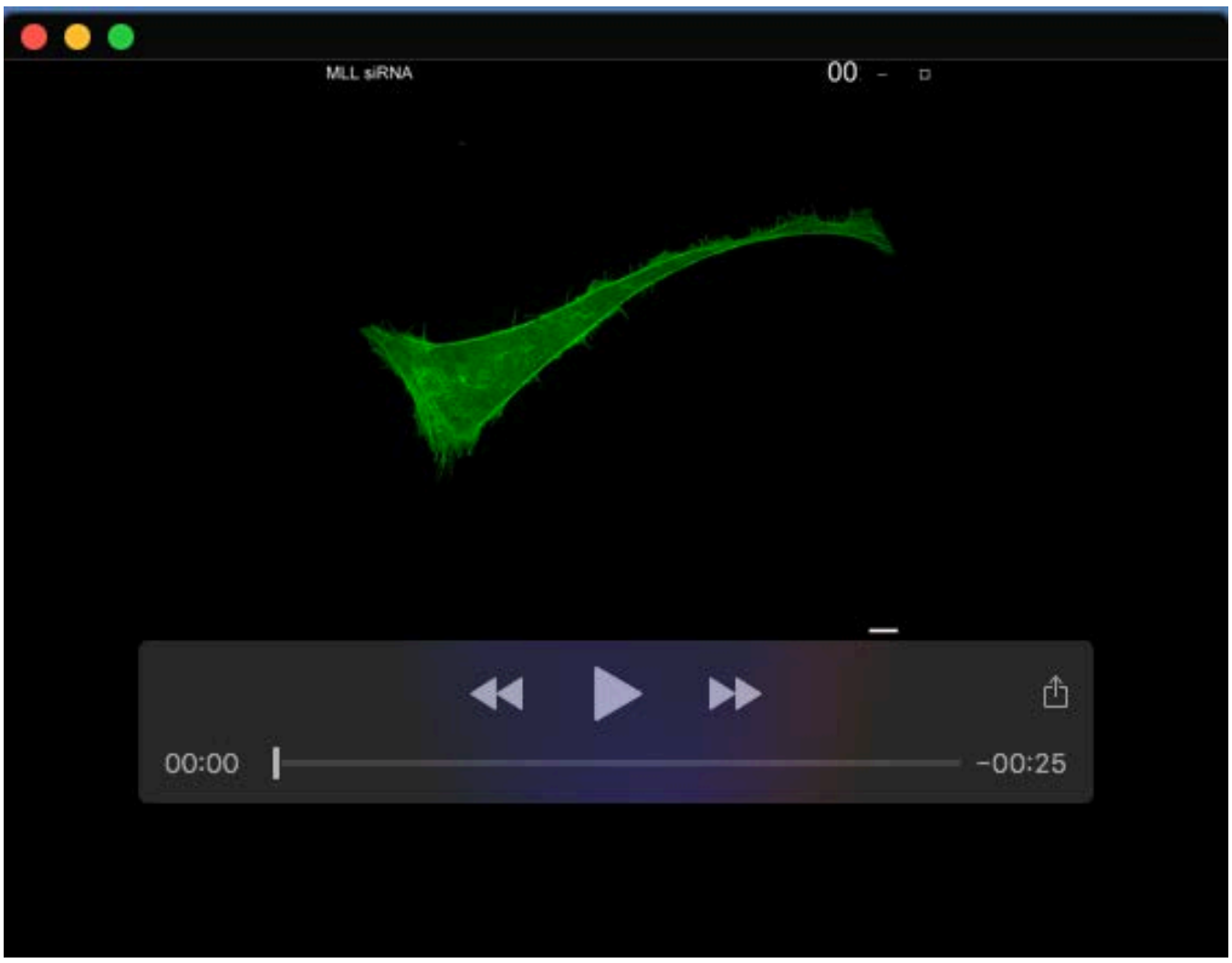

Movie 3. U-2OS cell expressing GFP-Lifeact (green) treated with MLL siRNA#1, corresponding to Figure 3G panel c is shown. Frame size is 128x128 µm and frame step is 5s. Scale bar, 10 µm.

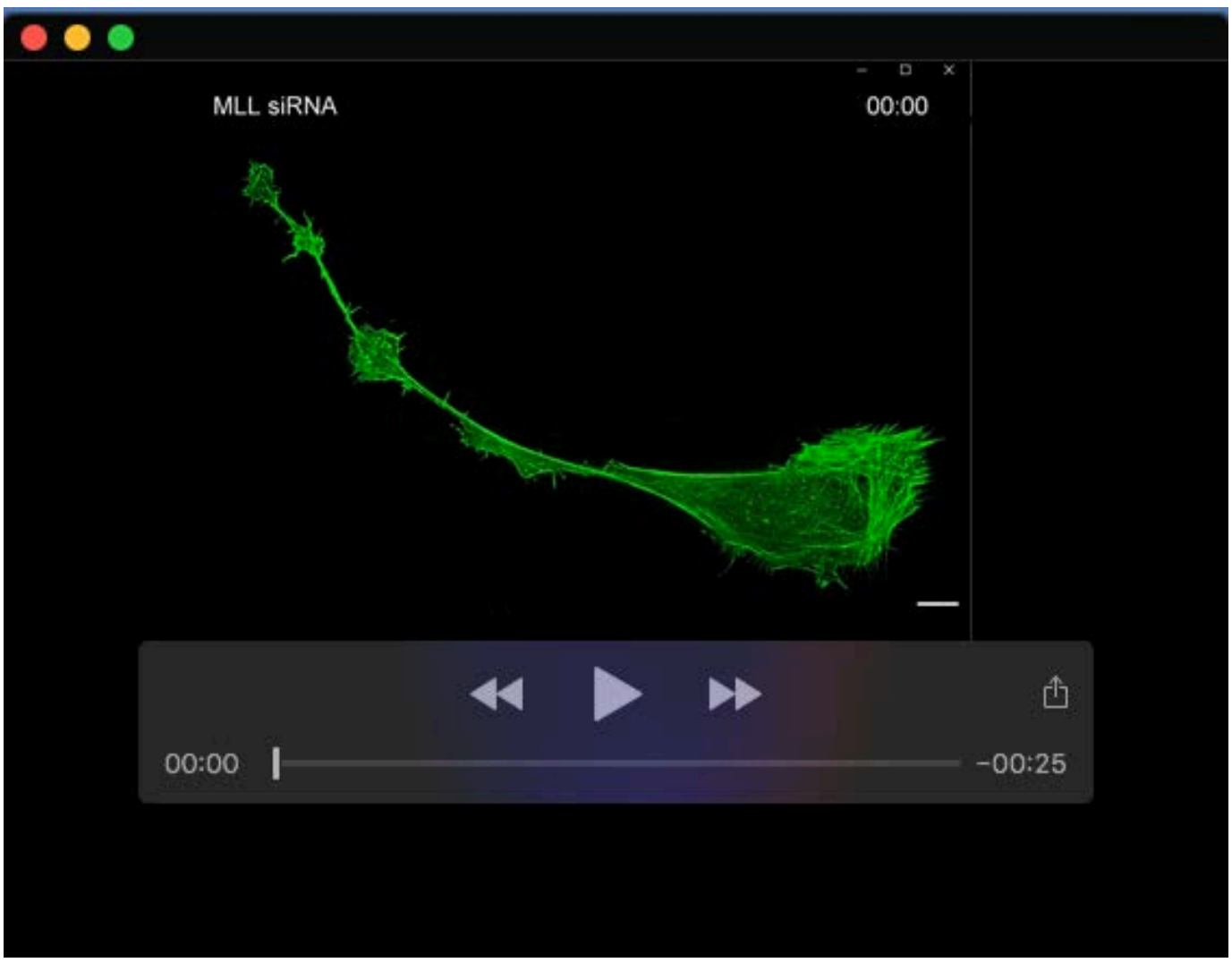

Movie 4. U-2OS cell expressing GFP-Lifeact (green) treated with MLL siRNA#1, corresponding to Figure 3G panel d is shown. Frame size is 186x130 µm and frame step is 5 s. Scale bar, 10 µm.